AMORPHOUS STRUCTURE CONTROLS MECHANICAL PROPERTIES OF JAMMED SOLIDS

by

FRANCESCO ARCERI

A DISSERTATION

Presented to the Department of Physics
and the Division of Graduate Studies of the University of Oregon
in partial fulfillment of the requirements
for the degree of
Doctor of Philosophy

September 2021

DISSERTATION APPROVAL PAGE

Student: Francesco Arceri

Title: Amorphous Structure Controls Mechanical Properties of Jammed Solids

This dissertation has been accepted and approved in partial fulfillment of the requirements for the Doctor of Philosophy degree in the Department of Physics by:

John Toner	Chair
Eric Corwin	Advisor
Ben Farr	Core Member
Marina Guenza	Institutional Representative

and

Andy Karduna	Interim Vice Provost for Graduate Studies

Original approval signatures are on file with the University of Oregon Division of Graduate Studies.

Degree awarded September 2021

DISSERTATION ABSTRACT

Francesco Arceri

Doctor of Philosophy

Department of Physics

September 2021

Title: Amorphous Structure Controls Mechanical Properties of Jammed Solids

A vast variety of physical systems falls within the description of amorphous solids. From glasses to grains, all of these materials share a disordered structure of their constituents. Understanding the nature of the mechanical properties of such systems is a conundrum which still poses challenging open questions. Recent experimental advances have led to the conclusion that the preparation of the system controls its stability against mechanical perturbations. In particular, amorphous solids can be classified as marginally stable or highly stable with respect to external perturbations. In this work I show that the amorphous structure, whether marginally or highly stable, uniquely controls the mechanical response of amorphous solids. First, I show that thermal glasses under very high pressure share the same mechanical and vibrational properties of athermal granular packings near the onset of rigidity. Secondly, I investigate the role of mechanical stability in the context of rheology, in particular with respect to cyclic shear training, and show that jammed solids are able to store an information of the repeated shear deformation only if the system, or a portion of it, is marginally stable.

This dissertation includes previously published and unpublished coauthored material.

CURRICULUM VITAE

NAME OF AUTHOR: Francesco Arceri

GRADUATE AND UNDERGRADUATE SCHOOLS ATTENDED:

University of Oregon, Eugene, OR, USA
University of La Sapienza, Rome, ITALY

DEGREES AWARDED:

Doctor of Philosophy, Physics, 2021, University of Oregon
Master of Science, Physics, 2017, University of La Sapienza
Bachelor of Science, Department of Physics, Physics, 2014, University of La Sapienza

AREAS OF SPECIAL INTEREST:

Soft Condensed Matter, Jamming, Rheology, Active Matter

PROFESSIONAL EXPERIENCE:

Research Assistant, University of Oregon, 2019-2021

Teaching Assistant, University of Oregon 2017-19

GRANTS, AWARDS AND HONORS:

Weiser Senior Teaching Assistant Award, UO Department of Physics, 2019

Weiser First Year Teaching Assistant Award, UO Department of Physics, 2018

PUBLICATIONS:

F. Arceri, E. I. Corwin, and Varda F. Hagh, "Marginal Stability Enables Memory Training in Jammed Solids" *arXiv preprint* arXiv:2106.05442 (2021)

F. Arceri, and E.I. Corwin, "Vibrational properties of hard and soft spheres are unified at jamming" *Phys Rev Letters* **112** (23) 238002 (2020).

F. Arceri, L. Berthier, G. Biroli, and F. Landes, "Glasses and aging: a statical mechanics perspective" *arXiv preprint* arXiv:2006.09725 (2020).

ACKNOWLEDGEMENTS

All of this work would not have been possible without the guidance of my advisor Eric Corwin. Special thanks go to Varda Faghir Hagh, the postdoctoral associate in my research lab, who I worked closely with for my latest project. I would like to express my gratitude to Giulio Biroli and Ludovic Berthier for giving me the opportunity of participating to the writing of the review article present in this dissertation, and to François Landes for a thriving peer collaboration. For various insights and support, I would like to thank my lab mates: James Sartor, Valerie Beale, Aileen Carroll-Godfrey, Cameron Dennis, Andrew Hammond and Jacob Hass. I would also like to thank my committee for their advice at various points throughout my graduate career. This work was supported by the NSF Career Award grant No. DMR-1255370, and the Simons Collaboration on Cracking the Glass Problem (No. 454939 E. Corwin)

To my family and friends who have always supported me.

TABLE OF CONTENTS

Chapter Page

LIST OF FIGURES

Figure Page

CHAPTER I

INTRODUCTION

When we think about a solid, the first thing that comes to mind is a rigid material where particles of the same shape are arranged in an ordered structure, in other words a crystal. Is this enough to describe all the solid systems around us? Surely, the answer is no. Despite real life crystalline solids are characterized by a variety of structural defects, countless physical systems do not feature a microscopic ordered structure but rather a disordered arrangement of their constituents. This class of materials falls under the definition of amorphous solids and the study of the mechanical properties of such systems is the object of this dissertation.

Examples of amorphous materials can be easily found in everyday life: from the sand on the ocean shore to the bubbles in the foam of dish soap, from window glass to flooring resins and many others. All of these materials are the result of a fast cooling or compression of a fluid, where particles had not had enough time to arrange into an ordered structure. Although this may sound reproducible only in an experimental laboratory, there is a pretty straightforward example which I invite the reader to think about: glass-blowing. Statues and ornaments made of glass are produced by blowing a molten material and shaping it to the desired look. A mixture of lead and silica glass is heated in a furnace at extremely high temperature until the glass becomes liquid. The glass-blower collects the heated glass through a pipe and blows air which expands the glass compound. This process needs to be quick since out of the furnace the glass rapidly solidifies. For this reason glass-blowers work next to the furnace so that they can heat up the glass to keep it malleable. This example shows that supercooling a liquid is a relatively easy task which can happen at room temperature and more importantly it highlights that the transition from liquid to glass is extremely rapid. From a physical point of view, the glass transition is defined as the point where the viscosity of the liquid exponentially increases above a certain threshold. Microscopically, particles cannot relax and find their preferred configuration but get stuck in a cage formed by their neighbors. As mentioned before, glasses are just one example of amorphous solids. In particular granular materials form another wide category of disordered solid systems. For a collection grains, rocks and so on, the average temperature that we experience throughout the year does not really effect their structure in an appreciable way. What controls

their solid state is the pressure under which they are confined. For example, let's imagine pouring sand inside a cylindric container. As we pour the sand, it behaves like a fluid and flows until the container is filled. If we now push our closed hand on the surface of the sand, we may be able to squeeze it initially but we quickly experience rigidity no matter how much we push further. The particles of sand block each other from flowing and the system pushes back against the applied pressure. This transition from fluid to solid behavior is called jamming.

Similarly to the glass transition, jamming is an out-of-equilibrium process where the constituents of the material get stuck in a disordered structure. However, jamming exclusively depends on how particles are arranged with respect to each other. By contrast, temperature fluctuations play an important role in the state of a system undergoing the glass transition. From a theoretical point of view, a glass can be produced starting from a liquid at equilibrium with its surroundings, and then by quenching it to a low temperature. If we imagine quenching a glass-former liquid down to zero temperature, the system will jam: the glass reaches a mechanically stable configuration in which all of the particles are stuck by their neighbors. Jamming is then a unifying point for the the physics of glasses and granular materials. Over the years, different models have been proposed to describe amorphous solids and among them, two extremely simple models have been greatly exploited: hard and soft sphere assemblies interacting through a pairwise potential. On one hand, a collection of hard spheres under a particular pressure and at a certain temperature is often used to describe glass-former liquids. In this model particles interact via colliding into one another and can be excited by thermal fluctuations. On the other hand, soft spheres are widely used to describe the physics of granular materials, systems where particles would deform under the forces exchanged with their neighbors. Soft spheres interact only when they are in contact and are allowed to overlap, occupying the same portion of space. The physical state of a soft sphere system is controlled by the competition between temperature and potential energy.

The hard and soft sphere models describe the jamming transition from two different perspectives. Firstly, let's imagine soft spheres under pressure in a confined box. The system can be decompressed by enlarging the volume of the box until there are just enough contacts between particles to ensure rigidity [3]. Secondly, by confining a collection of hard spheres in a box, particles will lock each other in an amorphous state and the system will become rigid.

If we imagine squeezing the box further, all the particles will eventually be forced to come into an enduring contact with their neighbors and the system will get stuck in a mechanically stable configuration [4, 5]. These two cases respectively represent approaching the jamming transition from above and from below the critical point. One could now ask: if I have a jammed configuration of hard spheres what happens if I switch on the soft sphere potential? In other words, are configurations of jammed hard spheres valid configurations of jammed soft spheres and vice versa? The answer is yes. Jamming is a purely geometrical transition which occurs when all the particles are constrained by a critical number of contacts. Furthermore, since jammed packings of soft and hard spheres share the same structure, do they also share the same mechanical properties? This question drove my research for the first part of my graduate career and in this dissertation I show that the mechanical properties of these two seemingly at odds models are unified at the jamming point. In particular the mechanical properties of extremely low temperature glasses and jammed granular solids are exclusively controlled by the amorphous structure.

What controls the amorphous structure of the system? Let's go back to the simple example of pouring sand into a container, but imagine putting a weight on top of the sand for a couple of hours. When we remove the weight and push on the surface, we find more resistance against squeezing the top layer of sand and we experience rigidity as soon as we touch it. Under the pressure of the weight, the sand particles have rearranged and reached a configuration which better supports an applied load, such as the weight of our hand. This configuration is more mechanically stable than the one we discussed before and it underlines the role of mechanical stability in defining the structure of the system. More stable configurations of jammed solids are able to support a bigger deformation, whether under pressure or shear stress. In particular, the rheology of a jammed solid is ruled by its mechanical stability [6]. While poorly stable jammed solids show a ductile behavior upon deformations, more stable amorphous configurations present a broad elastic response until a brittle failure, as for a shuttered window glass. Theoretically, amorphous solids in the vicinity of the jamming point are described as marginally stable: the arrangement in which particles are held in place is just enough to ensure mechanical stability so that a tiny mechanical perturbation leads the system to an instability. Recent advances in both experiments and computer simulations allow one to produce highly stable configurations of

amorphous solids. In particular it is now possible to tune mechanical stability and understand its influence on the mechanical response of the system. To this end, I recently explored the role of mechanical stability in the context of rheology of jammed solids. Furthermore, I studied the ability of these systems to adapt their mechanical response to a cyclic shear driving and store information of the repeated deformation in their structure, a property called memory training [7, 8]. This work leads to the conclusion that memory training is only possible when the system, or at least a portion of it, is marginally stable.

With this dissertation I show that the amorphous structure is exclusively responsible for the mechanical properties of jammed solids. Chapter II features a state-of-the-art description of the glass and amorphous states from a theoretical point of view. Here, the vibrational properties, jamming transition and rheology of amorphous solids are described. Chapter III focuses on the connection between thermal hard sphere glasses and granular materials at the jamming point, showing that the vibrational properties of hard and soft sphere systems are unified at jamming. Mechanical properties of the hard sphere model are explored using an effective energy potential which mimics the interaction between frequently colliding thermal hard spheres under very high pressure. Chapter IV explores the role of mechanical stability in the context of rheology and memory training by cyclic shear in jammed solids. Chapter II is available here [9] and it will be featured in the new edition of Encyclopedia of Complexity and Systems Science, Springer Edition. Chapter III has been published in Physical Review Letters [10] and Chapter IV is currently under review.

CHAPTER II

GLASSES AND JAMMING: A STATISTICAL MECHANICS PERSPECTIVE

Mean-field theory of the glass transition

In the last three decades, three independent lines of research, Adam-Gibbs theory [11], mode-coupling theory [12] and spin glass theory [13], have merged to produce a theoretical ensemble that now goes under the name of Random First Order Transition theory (RFOT), a terminology introduced by Kirkpatrick, Thirumalai and Wolynes [14, 15] who played a major role in this unification. Instead of following the rambling development of history, we summarize it in a more modern and unified way.

A key ingredient of RFOT theory is the existence of a chaotic or complex free energy landscape with a specific evolution with temperature and/or density. Analyzing it in a controlled way for three dimensional interacting particles is an impossible task. This can be achieved, however, in simplified models or using mean-field approximations, that have therefore played a crucial role in the development of RFOT theory.

A first concrete example is given by 'lattice glass models' [16]. These are models of hard particles sitting on a lattice. The Hamiltonian is infinite either if there is more than one particle on a site or if the number of occupied neighbors of an occupied site is larger than a parameter m, but is zero otherwise. Tuning the parameter m, or changing the type of lattice, in particular its connectivity, yields different models. Lattice glasses are constructed as simple statmech models to study the glassiness of hard sphere systems. The constraint on the number of occupied neighbors mimics the geometric frustration [17] encountered when trying to pack hard spheres in three dimensions. Numerical simulations show that their phenomenological glassy behavior is indeed analogous to the one of supercooled liquids [18–20]. Other models with a finite energy are closer to molecular glass-formers, and can also be constructed [21]. These models can be solved exactly on a Bethe lattice [1], which reveals a rich physical behavior [22]. In particular their free energy landscape can be analyzed in full details and turns out to have the properties that are also found in several 'generalized spin glasses'. Probably the most studied example of such spin glasses is the

[1] In order to have a well-defined thermodynamics, Bethe lattices are generated as random graphs with fixed connectivity, also called random regular graphs.

p-spin model, defined by the Hamiltonian [23]

$$H = -\sum_{i_1,\dots,i_p} J_{i_1,\dots,i_p} S_{i_1} \dots S_{i_p}, \tag{2.1}$$

where the S_i's are N Ising or spherical spins, $p > 2$ is the number of interacting spins in a single term of the sum, and $J_{i_1,\dots,i_p}$ quenched random couplings extracted from a distribution which, with no loss of generality, can be taken as the Gaussian distribution with zero mean and variance $p!/(2N^{p-1})$. In this model, the couplings $J_{i_1,\dots,i_p}$ play the role of self-induced disorder in glasses, and promotes a glass phase at low temperature.

All these models can be analyzed using the so-called replica theory [13]. Given its importance in setting the foundations of the theory of glasses at the mean-field level, we now present its main technical steps. To keep the discussion as simple as possible, we focus on p-spin models. Note that the theory holds for more complex models but it is technically more involved. The starting point is the computation of the free-energy which is obtained as an average over the distribution of couplings:

$$F = \lim_{N\to\infty} -\frac{1}{\beta N} \overline{\log Z_J}, \tag{2.2}$$

where $\overline{\cdots}$ represents the average over the disorder. Performing this average is possible thanks to the replica trick

$$\overline{\log Z_J} = \lim_{n\to 0} \frac{1}{n} \log \overline{Z^n}, \tag{2.3}$$

where n is the index of replicas, i.e. clones of the same system with different couplings $J_{i_1,\dots,i_p}$ extracted from the same distribution. The use of the replica trick may seem purely mathematical, yet it has a profound physical sense. If the system is ergodic, averages of thermodynamical observables for two replicas of the same system (with identical disorder) coincide, whereas they differ if ergodicity is broken. We can define the overlaps between two replicas a, b as Q_{ab}, which defines the $n \times n$ overlap matrix:

$$Q_{ab} = \frac{1}{N} \sum_{i=1}^{N} S_i^a S_i^b, \tag{2.4}$$

where the product between spins represents a dot product for spherical spins [24]. After some computations, the free energy can be expressed as a function of Q_{ab}, which therefore plays the

role of the order parameter. In the ergodic phase one expects symmetry between replicas [2], and the so-called replica-symmetic (RS) parametrization of Q_{ab} is adopted: all the off-diagonal elements of Q_{ab} are equal to $q_0 < 1$ and the diagonal elements are $Q_{aa} = 1$. The parametrization that corresponds to the glass phase, when ergodicity is broken, is the so-called one-step replica symmetry breaking (1RSB) solution. Here, the overlap matrix is divided into blocks of dimension $m \times m$; elements belonging to blocks far from the diagonal are equal to q_0, while off-diagonal elements of blocks along the diagonal are equal to q_1 with $1 > q_1 > q_0$. On the diagonal $Q_{aa} = 1$. This parametrization encodes the existence of many thermodynamically equivalent basins, hence two replicas can either fall in the same basin and have overlap q_1, or fall in two different basins and have overlap q_0. The crucial simplification introduced by the mean-field approximation is that barriers between basins have a free energy cost which grows exponentially with N, so that truly metastable states can be defined in the thermodynamic limit [25]. At high temperature (or low density) the RS solution has a lower free energy. Below the ideal glass transition temperature the 1RSB solution instead becomes dominant.

Liquids and glasses in infinite dimensions

A major theoretical breakthrough of the last years is the analysis of the glass transition for interacting particle systems in the limit of infinite dimensions [26–28]. The starting point approach is the definition of a pair interaction potential with a proper scaling with dimension d to ensure a non trivial thermodynamic limit:

$$v(r) = \tilde{v}[d(r/\ell - 1)] \tag{2.5}$$

where ℓ defines the range of the interaction. Many different potentials used to model glasses can be written in this way by using a suitable function $\tilde{v}(x)$, such as hard spheres, Lennard-Jones, Yukawa, square-well, harmonic, and Weeks-Chandler-Andersen potentials [28]. In the limit of infinite space dimension, $d \to \infty$, and using the scaling above, the thermodynamics and the dynamics of liquids and glasses can be analyzed exactly [3]. The resulting theory is qualitatively

[2] If additional symmetries are broken then one can have ergodicity breaking also in the RS phase.

[3] For large d the crystalline phase does not intervene. In fact, the amorphous and crystalline solid phases are well separated in configuration space and issues related to finite dimensions, such as the crystallization of monodisperse particles, are suppressed [29, 30].

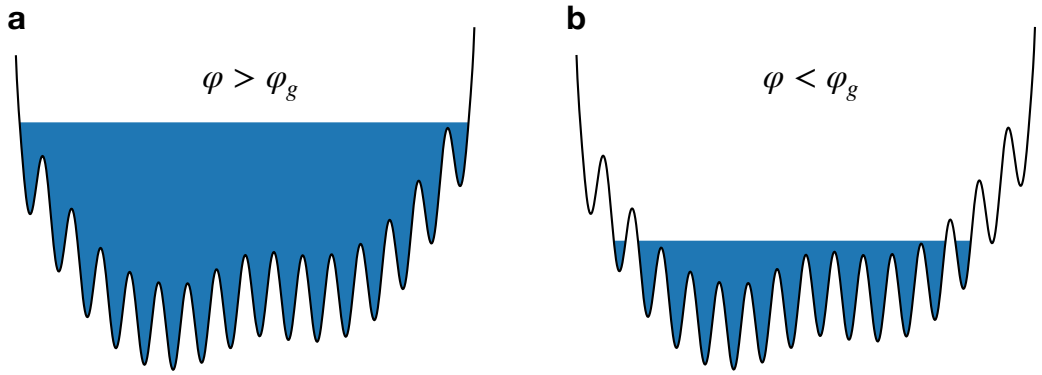

FIGURE 1. Sketch of the evolution of free-energy landscape of hard spheres across the glass transition. In the liquid phase (a) at low packing fractions $\varphi < \varphi_g$, every portion of the phase space is accessible. For $\varphi > \varphi_g$ the system is in the glass phase (b) and remains trapped in one of the many equivalent basins.

very similar to the one obtained from the simple models discussed in the previous section (both for the statics, in terms of replica formalism, and for the dynamics, in terms of self-consistent Langevin equations).

In fact, all these models belong to the universality class of 1RSB systems [31], with a free-energy landscape evolving as in the sketch in Fig. 1. At low densities or high enough temperatures, they all describe an ergodic liquid phase, analogous to the paramagnetic phase of a spin glass. Under cooling or application of an external pressure, the free energy breaks up into many different minima which eventually trap the dynamics, and the system enters the glass phase, as described further below.

The merit of the infinite dimensional theory is that it offers quantitative results and applies directly to microscopic models of liquids and glasses. Moreover, it directly reveals the nature of 'mean-field' theories and approximations, such as the diagrammatic liquid theory and Mode-Coupling Theory. Last but not least, it establishes once and for all that the 1RSB phase and associated physics and phase transition is the correct and universal mean-field theory of glass-forming models.

Mean-field theory of the amorphous phase

The phase transition between liquid and glass is not the only interesting phenomenon characterizing the phase diagram of glassy materials. Since the transition occurs at finite

pressure and temperature, glasses can be further compressed or cooled within the glass phase itself [26, 27, 32]. How do physical properties of glasses change in this context? In mean-field theory, this question has been widely investigated by using the hard spheres glass model [33, 34], a favorite canonical example of a glass-former system because of its analytical simplicity. Eventually, by compressing a hard sphere glass, the system undergoes the jamming transition in the limit of infinite pressure [5]. In this section, we briefly survey recent progress in the development of an analytic theory of the glass phase in the large d limit, with a particular emphasis on hard spheres [28].

Mean-field glassy phase diagrams

When a glass-forming liquid undergoes the glass transition, it becomes confined into a single free energy minimum and the timescale to explore different minima becomes infinite. It is formally possible to define thermodynamic properties by restricting the available statistical configurations to a single free energy minimum. This can be enforced in the replica formalism by considering two copies of the system and constraining the distance between them [2]. First, an equilibrium reference configuration $\underline{Y}$ at $(T_g, \hat{\varphi}_g)$ is introduced, where $\hat{\varphi}$ is the scaled packing fraction $\hat{\varphi} = 2^d\varphi/d$. Second, a copy of the equilibrium configuration $\underline{X}(t)$ is created and evolved in time. Let us define now the mean-squared displacement (MSD) between the two copies as $\overline{\langle\Delta(\underline{X},\underline{Y})\rangle} = \Delta_r$. The properties of $\underline{X}(t)$ are sampled in a restricted region of phase space close to the equilibrium configuration. Within this state following construction, the system at $(T_g, \hat{\varphi}_g)$ with initial configuration $\underline{Y}$ can be adiabatically followed anywhere in the glass phase diagram.

Concretely, for the glass state selected by $\underline{Y}$ and followed until $(T, \hat{\varphi})$, we can write the restricted partition function as:

$$Z[T, \hat{\varphi}|\underline{Y}, \Delta_r] = \int d\underline{X} e^{-\beta V(\underline{X})} \delta(\Delta_r - \Delta(\underline{X}, \underline{Y})), \tag{2.6}$$

where $V(\underline{X})$ is the potential energy of the configuration $\underline{X}$, and the delta function enforces the restricted average. In order to obtain the glass free energy, we need to compute its average over

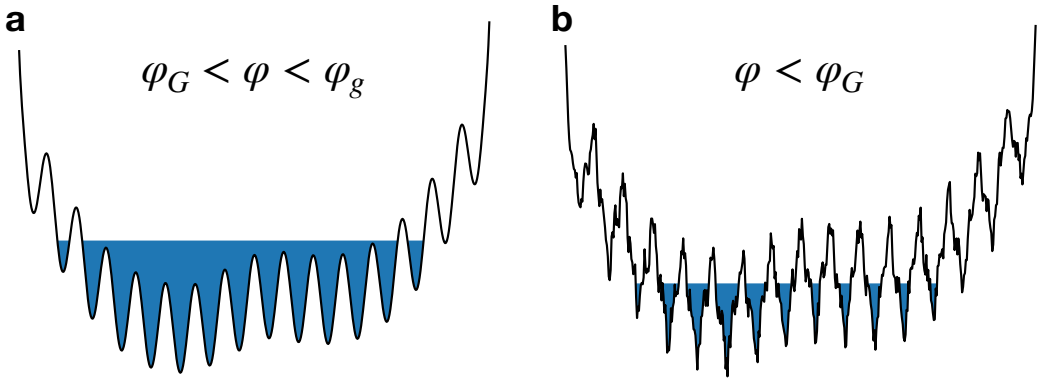

FIGURE 2. (a) Sketch of the free energy structure deep in the hard sphere glass phase, where each basin breaks down in sub-basins corresponding to secondary relaxations. At the Gardner transition in (b), the sub-basins become fractal and ergodicity is broken.

the chosen reference configuration $\underline{Y}$, which acts as a source of quenched disorder:

$$f_g(T,\hat{\varphi}|T_g,\hat{\varphi}_g,\Delta_r) = -\frac{T}{N}\int \frac{d\underline{Y}}{Z[T_g,\hat{\varphi}_g]} e^{-\beta_g V(\underline{Y})} \times \ln Z[T,\hat{\varphi}|\underline{Y},\Delta_r] \tag{2.7}$$

where $Z[T_g,\hat{\varphi}_g] = \int dY \exp^{-\beta_g V(\underline{Y})}$ is the partition function at $(T_g,\hat{\varphi}_g)$. Mathematically, the quenched disorder is handled using the replica method. We then introduce $(n+1)$ replicas of the original system, with the initial glass at $(T_g,\hat{\varphi}_g)$ being the master replica, while the n other slave replicas describe the glass at $(T,\hat{\varphi})$. The glass free energy is finally expressed in terms of the average MSD between the slave replicas and the master replica Δ_r, and the average distance between the slave replicas Δ. At this step, we assume that the symmetry between slave replicas is not broken, which corresponds to the 1RSB ansatz previously described.

By choosing the state point at $(T,\hat{\varphi}) = (T_g,\hat{\varphi}_g)$, the recursive equations for Δ and Δ_r have to satisfy $1/\hat{\varphi} = \mathcal{F}_\beta(\Delta)$, where $\mathcal{F}_\beta(\Delta)$ is a positive function which vanishes for both $\Delta \to \infty$ and $\Delta \to 0$, with an absolute maximum in between. This equation can then be satisfied only if

$$\frac{1}{\hat{\varphi}_d} \leq \max_{\Delta} \mathcal{F}_\beta(\Delta). \tag{2.8}$$

This condition occurs for volume fractions larger than a critical value $\hat{\varphi}_d(\beta_g)$, which corresponds to the dynamical glass transition.

We can explore the glass phase following the glass prepared at the glass transition $(T_g, \hat{\varphi}_g)$ at different temperatures and packing fractions. At low T and high $\hat{\varphi}$ one eventually meets another phase transition, where the 1RSB assumption fails [13] and the more complex full-replica symmetry breaking (fullRSB) solution is necessary to compute the glass free energy, the so-called Gardner phase transition [35, 36]. Here, the fullRSB solution corresponds to a hierarchical organization of the distances between the slave replicas and the glass becomes marginally stable [37, 38]. The emergence of a complex free energy landscape gives rise to non-trivial dynamical processes [39–41]. A pictorial representation of the Gardner transition is shown in Fig. 2.

It is worth noting that the derivation sketched above is completely general and can be used for any glassy pair potential mentioned in the previous section. In the following we will apply this formalism to the hard spheres model, for which several implications from the mean field picture have been successfully tested numerically [31, 42]. Here, the relevant state parameter is the scaled reduced pressure $\hat{p} \equiv \beta P/\rho d$.We refer to Refs. [32, 36, 41, 43] for more results regarding systems made of soft potentials.

Starting from an equilibrated hard sphere liquid configuration at $\hat{\varphi}_g$, we can apply the state following formalism to explore the hard sphere phase diagram in Fig. 3. The reduced pressure can be computed from the equation of state of an infinite dimensional hard sphere liquid $\hat{p} \sim \hat{\varphi}/2$, derived from h Virial expansion of the free energy [44]. Starting from $\hat{\varphi}_g$ and decompressing the system, the glass eventually undergoes a melting transition: the 1RSB solution becomes unstable and the glass melts into the liquid via a spinodal instability [27]. Upon compression instead, the glass enters deeper into the glass phase and remains dynamically arrested. Numerically, this has been proven by measuring Δ as the long-time limit of the MSD $\Delta(t)$ between the system at time t and the initial configuration at $t = 0$. The order parameter of the transition Δ_r is instead computed as the long-time limit of the distance $\Delta_{AB}(t)$ between two copies A and B of the same initial system evolved with different initial velocities:

$$\Delta_{AB} = \left\langle \frac{1}{N} \sum_{i=1}^{N} |\mathbf{r}_i^A - \mathbf{r}_i^B|^2 \right\rangle . \tag{2.9}$$

Upon further compression, the glass eventually undergoes the Gardner transition at a finite pressure $\hat{p}_G$. Here, the relation between Δ_r and Δ breaks down and $\Delta(t)$ is characterized by a

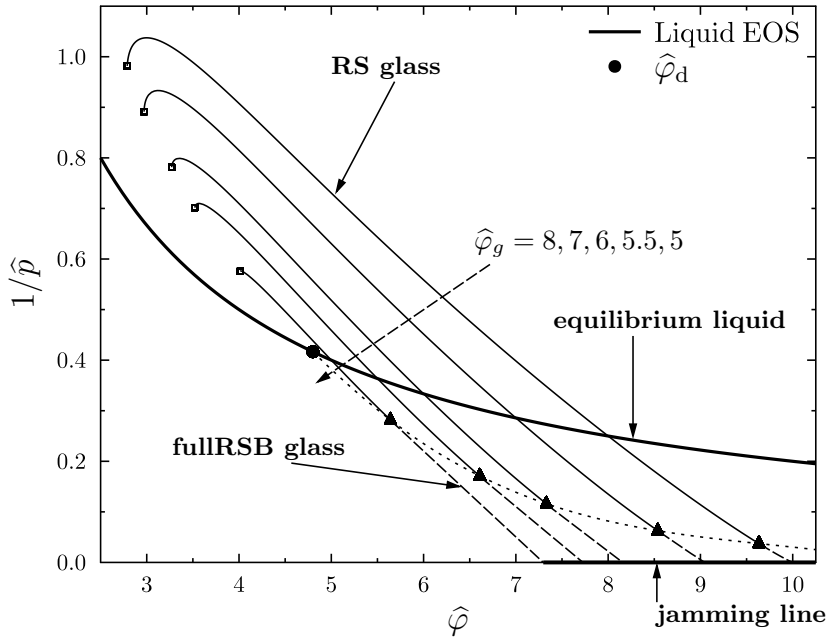

FIGURE 3. Phase diagram of hard spheres in the inverse reduced pressure – reduced packing fraction $(1/\hat{p}, \hat{\varphi})$ plane. The glass transition is marked by a full circle. The glass equations of state are reported as full lines in the region where the replica symmetric solution is stable. The Gardner transition is marked by triangles, beyond which the fullRSB solution is stable (dashed lines). The glass equations of state end at the jamming transition. Upon decompression, glasses are stable until a spinodal instability arises (open squares).

logarithmic growth in time, suggesting the emergence of a complex free energy landscape [42]. The copies A and B cannot occupy the same sub-basin and are no longer able to explore the entire metabasin. Due to the fractal nature of the free energy landscape, the excitations required to move around the fractal states correspond to soft modes [41]. The correlation length of these modes can be estimated by measuring the dynamical susceptibility, computed as the variance of Δ_{AB}, which indeed shows a divergence at the Gardner transition [42].

Compressing further within the Gardner phase, the pressure eventually diverges as the system reaches its jamming density $\hat{\varphi}_J$, which depends explicitly on the selected initial condition $(T_g, \hat{\varphi}_g)$. In particular, there exists a range of jamming points, or a 'jamming line' [45], whose extension increases with d [26].

Jamming

During the last two decades, a large research effort has shed light on the critical behavior characterizing the jamming transition [46]. Jamming can be seen from two different perspectives. An assembly of Brownian hard spheres under compression becomes rigid at a finite density, at which point the pressure diverges. On the other hand, athermal packings of soft repulsive spheres reach the jamming point under decompression when the pressure vanishes. In both situations, each particle is constrained by enduring contacts with the neighbor particles and the system is rigid. In particular, at jamming the average number of contacts per particle Z reaches the critical value $Z_c = 2d$, which represents the lower limit for mechanical stability [47] (Maxwell's criterion for rigidity). From the hard spheres side, Z jumps from zero to Z_c at the transition, while from the soft spheres side, as the pressure decreases toward zero the excess number of contacts scales as [3, 48]:

$$\Delta Z \equiv Z - Z_c \sim \Delta\varphi^{1/2}, \tag{2.10}$$

where $\Delta\varphi = \varphi - \varphi_J$ is the amount of compression above the jamming threshold. A connection between hard and soft spheres at jamming is observed in the pair correlation function [3, 4], confirming that allowed configurations of hard and soft spheres are identical at jamming.

When $\Delta Z = 0$ the system is isostatic, i.e. there are just enough contacts to ensure mechanical stability and the system is marginally stable: breaking a bond between contacts can lead to an excitation that causes a collective motion throughout the whole system [49]. Not surprisingly, this critical behavior fits well into the free energy picture of marginal glasses reported above.

Marginality in athermal jammed solids can be explained in real space by the so-called cutting argument [50]. Imagine removing the contacts between a subsystem of linear size l and the rest of the system. If we slightly compress the system, this cutting will lead to a competition between the overall excess contacts ΔZ created by the compression, and the missing contacts at the boundary of the subsystem. If the total number of contacts is below the isostatic value $N_{iso} = NZ/2$, then there are modes with no energetic cost, i.e. soft modes. The number of soft modes N_{soft} then corresponds to the difference between the number of contacts at the boundary, proportional to l^{d-1}, and the number of extra contacts created by the compression, which scales

as $\Delta Z l^d$. There is then a critical length $l^* \sim \Delta\varphi^{-1/2}$ for which the system looks isostatic and for $l = l^*$, soft modes correlate over the whole subsystem. These extended anomalous modes correspond to random excitations over all the system, profoundly different from acoustic modes proper of crystalline solids.

Other anomalies of jammed solids are observed in the scaling of the elastic moduli near the transition. These critical behaviors have been successfully described within a force network picture, for which en effective medium theory has been developed [51, 52]. In particular, a jammed soft sphere configuration can be mapped onto a network of springs with elastic contacts k_{eff}, computed as second derivatives of the pairwise interaction between particles. The resulting scaling behaviors for the bulk modulus $B \sim k_{eff}$ and the shear modulus $G \sim k_{eff}\Delta\varphi^{1/2}$ suggest that the Poisson ratio $G/B \sim \Delta\varphi^{1/2}$ vanishes at the jamming transition [3]. This criticality reflects on the frequency of normal modes which is directly related to the elastic moduli $(B(\omega), G(\omega))$ by the dispersion relation $\omega^* = ck^*$, where $k^* \sim 1/l^*$ and c is the speed of sound. Since sound propagates either longitudinally (B) or transversely (G), two different length scales can be defined: the longitudinal length scale $l^* \sim \Delta\varphi^{-1/2}$, which matches the cutting length scaling behavior and is indeed attributed to extended soft modes, and the transverse length scale which follows the scaling $l_t \sim \Delta\varphi^{-1/4}$.

Other critical scaling laws have been predicted both by replica mean field calculations and effective medium theory for a spring network, with good consistency with numerical results in finite dimensions. In particular, the distributions of interparticle voids and interparticle forces follow universal power-laws [53–56]. Contact forces can be either extended or localized, with distributions defined by power law exponents θ_e and θ_l respectively. Extended forces are predicted from the infinite dimensional exact solution, whereas the localized forces likely result from the presence of localized defects, such as rattling particles, which only exist in finite dimensions. Remarkably, the numerical value of the critical exponents associated to scaling laws near jamming can be predicted analytically in the mean-field approach [28], and their value is confirmed by numerical simulations in dimensions $d \geq 2$.

The influence of temperature on the jamming criticality has also been studied [52, 57]. These works show that above jamming there exists a region in the plane $T-\varphi$ where the harmonic approximation of the soft sphere potential holds, and the vibrational spectrum converges to its

zero temperature limit, provided that $T < T^*(\varphi)$. The value of $T^*(\varphi)$ decreases with $\Delta\varphi \to 0$ with a trivial scaling exponent. A similar result holds below jamming for hard sphere glasses [58]. For $T > T^*(\varphi)$, the harmonic approximation breaks down, defining an anharmonic critical regime, controlled by non-analyticities in the interparticle potential. Physically, strong anharmonicities stem from the constant breaking and reformation of particle contacts in the presence of thermal fluctuations [59].

Vibrational properties

The anomalous thermal properties of low temperature glasses can be related to the structure of the free energy landscape of glassy states. Amorphous solids behave very differently from crystalline solids. In terms of heat capacity and thermal conductivity, crystals are dominated by phononic excitations with a low-frequency density of states (DOS) $D(\omega)$ given by the Debye scaling law $D(\omega) \sim \omega^{d-1}$. Instead, the thermal properties of glasses are dominated by an excess of vibrational modes referred to as the boson peak and by an anomalous low-frequency scaling of $D(\omega)$. This excess of anomalous vibrations reflects, within mean-field theory, the existence of multiple free energy barriers in glassy states. In fact, when the glass enters the Gardner phase, the system becomes marginal and even infinitesimal perturbations lead to excitations that can bring the system to a different glassy state.

The mean-field theory of glasses has been explored using soft spheres in the jamming limit [60]. The theory predicts the low-frequency scaling of the vibrational density of states (vDOS) to be $D(\omega) \sim \omega^2$ in any dimension [34, 51, 61], quite differently from the Debye scaling. The same result was previously obtained within the effective medium theory [55].

Numerically, the nature of the low-frequency vibrational spectrum has been widely studied using soft spheres packings close to jamming. Early studies suggested the existene of the $D(\omega) \sim \omega^2$ scaling [31, 60] for a wide range of dimensions d, reinforcing the relevance of the mean-field description for finite dimensional systems [62]. The modes giving rise to this scaling form have been found to be extended anomalous modes. A more recent study established that the ω^2 scaling is only observed over a finite frequency range, which seems to increase systematically with the space dimension d, which is consistent with a pure quadratic scaling when $d = \infty$. However, for any finite d, the density of states eventually obeys Debye scaling for sufficiently low frequencies.

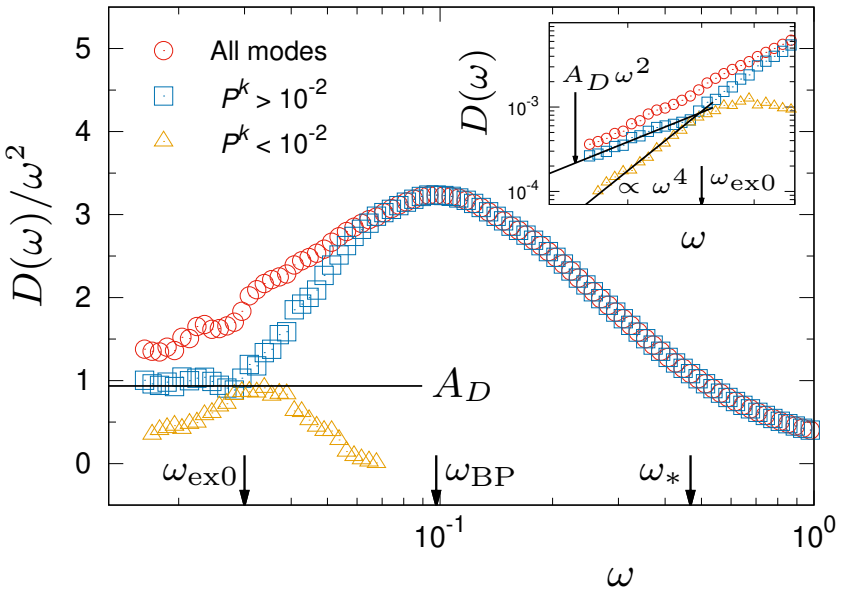

FIGURE 4. Adapted from [1]. Vibrational density of states of jammed harmonic soft spheres scaled by the Debye law ω^{d-1} in $d = 3$. Modes with index k are classified as extended (blue) or localized (yellow) by their participation ratio P^k. Below the boson peak frequency ω_{BP}, the density of states is the superposition of anomalous extended modes eventually obeying Debye scaling, and a population of quasi-localised modes scaling as ω^4, as confirmed in the inset.

Finally, recent numerical works show that for frequencies lower than the boson peak, an additional family of soft modes due to marginal instabilities can be observed [1, 63]. As Fig. 4 shows, the vibrational density of these additional modes scales as ω^4. A spatial analysis of such modes shows that they correspond to quasi-localised modes, which are again absent from the large d analytic description.

Rheology

Once the glass is created, it can be adiabatically cooled or compressed, but it can also be deformed by applying an external mechanical constraint. The rheology of amorphous solids is a very broad research field. Here, we present recent results in this field obtained using the mean field glass theory, including implications regarding elasticity, yielding and shear jamming [37, 64, 65].

We report results obtained from the same state following formalism applied to study the amorphous phase along a compression in the $d \to \infty$ limit. If the master replica $\underline{Y}$ is in the

dynamically arrested region, the system reacts elastically to a small applied strain γ. We can then obtain the stress-strain curve as a function of the state point $(T, \hat{\varphi})$ of the slave replica $\underline{X}$. The stress for an elastic medium increases linearly with strain, which defines the shear modulus $\hat{\mu} = \frac{d\hat{\sigma}}{d\gamma}$ computed at zero strain, where stress and shear modulus are scaled such that the $d \to \infty$ limit remains finite. In the small strain limit one finds

$$\hat{\mu} = \frac{1}{\Delta} \tag{2.11}$$

where Δ is the long time limit of the MSD. The MSD $\Delta(\underline{X}, \underline{Y})$ is the superposition of an affine component due to the strain, and of a non-affine contribution defined by the particular shear protocol. At the glass transition, the shear modulus jumps from a zero value (liquid state) to a finite value at $\hat{\varphi}_d$ (glass state). In finite dimensions, this sharp discontinuity becomes a crossover [28].

When the system is confined within a glass state, it is able to sustain a shear strain on a time scale which corresponds to the diverging time scale for which the dynamics becomes diffusive. One can then follow adiabatically the slave replica until a state point $(T, \hat{\varphi})$ and study the linear response to shear for the different phases of the glass. This corresponds to exploring the strain vs volume fraction phase diagram of the system. Upon decompression, the shear modulus decreases and displays a square root singularity at the melting spinodal point [28, 64].

Increasing the strain and/or the volume fraction, the glass phase may undergo a Gardner transition and transform into a marginal glass, for which all non-linear elastic modulii diverge and standard elasticity theory does not hold anymore [66]. As for a simple compression without shear, the boundary of the Gardner phase transition explicitly depends on the selected glass state.

Once the Gardner phase is entered, upon further compression or strain, two kinds of transition may occur in hard sphere glasses. First, the shear modulus may increase and eventually diverge when a jamming point is reached. At zero strain, this is the ordinary jamming transition. In that case, the power law scaling of the MSD directly implies a similar behaviour for the shear modulus. In the presence of a finite strain, this corresponds to the phenomenon of shear jamming, observed in the context of granular materials [67, 68].

A second type of instability can occur when increasing the strain of a hard sphere glass. Here, the shear stress reaches a maximum followed by a spinodal instability where the fullRSB

solution for Δ and Δ_r is no longer stable. The spinodal point $\gamma_Y(\hat{\varphi}_g)$ corresponds to the glass yielding transition [67, 69]. The yielding transition in glasses has been studied for a variety of models and under different physical conditions [70, 71]. In particular, it has been suggested that the yielding transition belongs to the same universality class as the RFIM, i.e. a spinodal transition with disorder.

Acknowledgments

We thank all the collaborators who worked with us on glass physics. This work was supported by a grant from the Simons Foundation (Grant No. 454933, L. B., Grant No. 454935, G. B.)

CHAPTER III

VIBRATIONAL PROPERTIES OF HARD AND SOFT SPHERES ARE UNIFIED AT JAMMING

Introduction

Glasses and granular materials are unified by their expression of amorphous rigidity. Seen from the perspective of soft sphere granular systems, described as soft sphere packings, jamming marks the onset of rigidity and occurs at zero pressure, when every particle becomes fully constrained but all contacts are just kissing [47]. By contrast in hard sphere glasses, considered as shadow systems for colloidal glasses [72], rigidity is achieved at the dynamical glass transition [73, 74] and the jamming point is only reached at infinite pressure when all the particles are forced to come into enduring kissing contact with one another [2]. As such, the jamming point is a matching point for the two systems, where hard sphere glasses end and soft sphere rigid solids begin. Even though the configurations found in each limiting case must be valid configurations for the other, there is no *a priori* reason to expect that the properties of such configurations should bear any meaningful relation due to their very different origins and interactions. Although the criticality of jamming has been explored from both hard and soft sphere perspectives [42, 54, 75], whether the jamming point represents a smooth crossover between hard and soft spheres or a singular point is still an open question. In this work we demonstrate that the vibrational properties of both hard and soft sphere systems approach the jamming transition point in the same manner and show no discontinuity between behavior below and above jamming. We use an effective potential to bring packings of hard spheres to their free energy minima, allowing us to quench towards jamming without the limitations of conventional thermal simulations and to directly measure the vibrational spectrum from the dynamical matrix.

Amorphous solids exhibit vibrational properties very different from those predicted by Debye theory [76–78]. The replica mean field theory of glasses and jamming predicts the low-frequency scaling of the vibrational density of states (VDOS) to behave as $D(\omega) \sim \omega^2$ for systems in every spatial dimension [34, 51, 60, 61]. This non-Debye scaling has been observed numerically in systems of soft spheres right above the jamming point [62] and is the result of an excess of vibrational modes within this low frequency range. These excess modes are spatially

extended but non-phononic and give rise to a peak in the heat capacity of glasses, often called the boson peak [79–81]. The VDOS associated with these modes is nearly flat for low frequencies ranging down to a crossover frequency ω^* below which it decays to zero [3]. At jamming even an infinitesimal excitation leads to an extended motion and the VDOS is flat until $\omega^* = 0$ [82].

In contrast to the mean field picture, as low dimensional soft sphere systems are brought to densities above jamming an additional class of modes appears as quasi-localized modes which are hybridized between system spanning phonons and local rearrangements [1]. These modes are believed to control the elastic response to externally applied shears [6, 83] and are measured to follow a low frequency scaling of $D_{loc}(\omega) \sim \omega^4$ [63, 84–86]. Such a scaling result has been observed for a wide variety of disordered systems [87–89]. These quasi-localized modes do not appear in the mean field picture as they are exclusively a low-dimensional phenomenon [90].

Similar quasi-localized modes play a central role in the physics of real low-temperature glasses [56, 57]. They are described as soft excitations that connect two local minima of the free energy, a scenario introduced by Phillips in the two-level tunneling model [91, 92]. These modes can be derived from anharmonic effects which are directly related to the non-analytic form of the hard sphere potential [57, 93–95]. Anharmonic effects independently arise from perturbation theory of hard spheres near jamming [60, 96], where the free energy has been found to be well approximated by a logarithmic effective pair potential [97] and higher order corrections to this behavior are unnecessary even at a finite distance to the jamming point [98]. The same effective interaction has also been shown in simulations of thermal hard spheres under very high pressure [58] for which an effective medium theory has been developed [52].

In the limit of high pressure thermal hard spheres this effective logarithmic potential can be understood as deriving from entropic consideration. If the typical timescale between collisions is much smaller than the typical timescale for relaxational rearrangements then the time-average of the momenta exchanged between frequently colliding particles is inversely proportional to the gap h between those particles [58]. This coarse graining over time defines a network of effective forces between hard spheres with corresponding potential energy given by a sum of two-body logarithmic potentials of the form

$$V(h) = -k_B T \log(h). \tag{3.1}$$

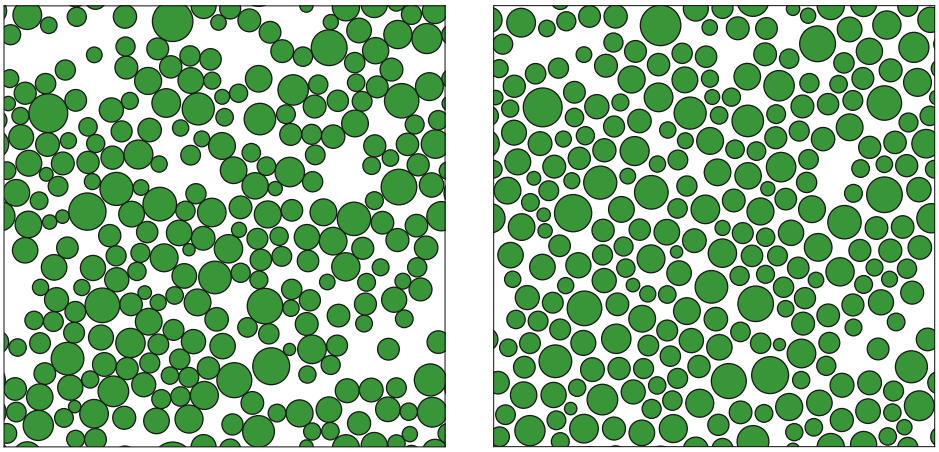

FIGURE 5. Minimization of the effective logarithmic potential in $d = 2$ with packing fraction $\varphi = 0.55$. Left: packing after harmonic minimization. Right: final configuration of the same packing after the logarithmic potential minimization.

Thermal hard spheres near jamming can thus be directly mapped to a collection of athermal particles interacting via the logarithmic effective potential.

While the mean field theory predicts the same vibrational properties for hard spheres below jamming and soft spheres above jamming, in low dimensional systems the vibrational spectra could be very dissimilar due to the very different circumstances giving rise to quasi-localized modes. In this paper, we present a protocol to produce stable glassy configurations based on the minimization of the effective free energy potential for a packing of athermal hard spheres. By measuring the evolution of the vibrational spectrum approaching jamming we show that the spectrum of jammed solids is unified when crossing the transition between the hard and the soft sphere descriptions. This result demonstrates that mechanical and thermal properties of jammed solids arise purely from a geometric origin.

Numerical methods

Hard sphere packings are produced using the pyCudaPacking package, developed by Corwin *et al.* [54, 99]. The packing is a collection of N particles in $d = 2, 3$ spatial dimensions, with a log normal distribution of particle sizes chosen to avoid crystallization. The packing is inside a box of unit volume with periodic boundary conditions and characterized by the packing fraction φ, the fraction of the box volume occupied by particles.

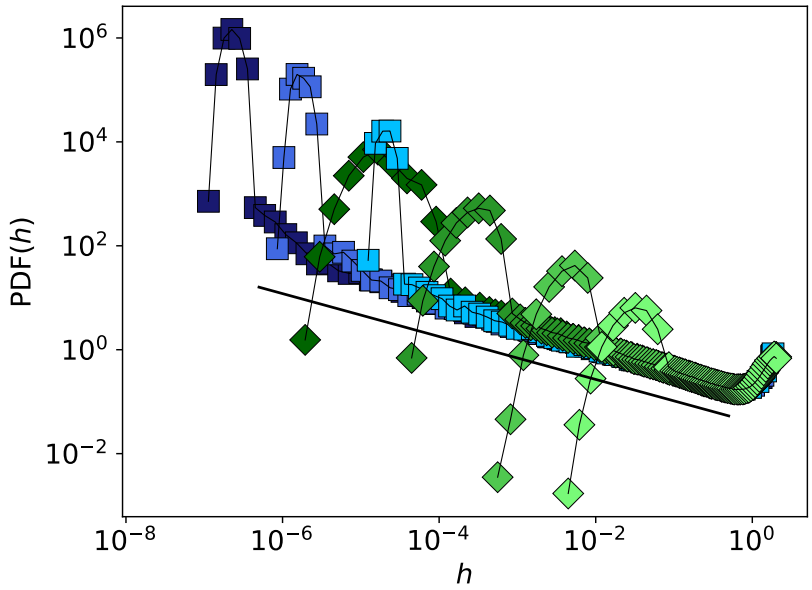

FIGURE 6. Gap distribution of hard sphere packings in $d = 3$. The distance from jamming increases from left to right: data from decompressions (blue squares) $\Delta\varphi = 1.1 \times 10^{-7}, 1.3 \times 10^{-6}, 1.5 \times 10^{-5}$, data from compressions (green diamonds) $\Delta\varphi = 2.3 \times 10^{-5}, 2.1 \times 10^{-4}, 3 \times 10^{-3}, 2 \times 10^{-2}$. The distributions peak around the value of the typical nearest neighbor gap and then decay following a power law scaling (black line) consistent with the mean field prediction $h^{-\gamma}$ with $\gamma = 0.41296...$ [2]. Gaps are cutoff at $h = 1$ to avoid showing next nearest neighbor behavior.

Starting from a packing fraction well below jamming we randomly distribute particles and minimize energy using a harmonic interaction potential (the same as used in the context of soft spheres [48]) to eliminate any overlap between particles. The logarithmic potential is then applied as a pair potential between particles separated by less than a cutoff gap distance. This cutoff is chosen to be twice the value of the position of the first peak of the gap distribution to allow for nearest neighbor interactions and exclude the non-physical next nearest neighbor interactions. However, all the results reported herein are insensitive to this choice as long as the cutoff encompasses nearest neighbors, see Supplementary Materials. We then minimize the potential using the FIRE (Fast Inertial Relaxation Engine) algorithm [100].

The result of the minimization of the logarithmic potential is depicted in Fig. 5. From an initial packing characterized by a broad distribution of nearest neighbor gaps, the system reaches a configuration where the nearest neighbor gaps are more uniform. This resulting packing is compatible with the time-averaged limit of a thermal hard sphere system, where collisions push

particles as far as possible from their neighbors on average [58]. If φ is less than the jamming packing fraction φ_J, no particles are in contact after the minimization and a void region can be found around each particle. We exploit this to creep up in density by inflating particles until saturating 10% of the minimum gap and then minimizing the effective potential for this new packing fraction. Repeating this procedure iteratively we are able to push the system to a distance from jamming $\Delta\varphi = |\varphi_J - \varphi|$ of the order of 10^{-6}. To produce packings at densities significantly closer to jamming, we decompress critically jammed soft sphere configurations and then minimize the logarithmic potential [54]. By slightly decompressing these packings we maintain the same spatial structure of the jammed systems, with a precise tuning of the distance from jamming $\Delta\varphi$.

Fig. 6 shows the gap distribution from both compressions and decompressions exhibiting the same behavior. We find a power-law scaling of the gap distribution that is well described by the mean field scaling law $\mathrm{PDF}(h) \propto h^{-\gamma}$ [2] and has previously been measured for soft spheres precisely at jamming [54]. The systems created by decompression from jamming show a sharper peak for the nearest gaps than is found in systems created through compression, even when both systems are nearly the same distance from the jamming transition. This reflects the underlying property that systems created from jammed soft spheres will maintain a memory of their kissing contacts, while those compressed from below have not yet chosen a single set of incipient contacts and thus have a broader distribution. Nevertheless, for every protocol, the distribution of nearest gaps tends to a delta function upon approach to the jamming point as the nearest neighbors become contacts.

Vibrational spectrum analysis

In order to distinguish extended and localized modes we compute the participation ratio (PR) of each mode, a measure of the fraction of particles that are participating in the motion governed by the mode. Given a mode at frequency ω with eigenvectors $\{\mathbf{u}_i(\omega)\}$, where $\mathbf{u}_i$ is the displacement vector for particle i, we define the PR as:

$$\mathrm{PR}(\omega) = \frac{1}{N_s} \frac{(\sum_i^{N_s} |\mathbf{u}_i(\omega)|^2)^2}{\sum_i^{N_s} |\mathbf{u}_i(\omega)|^4} \ , \tag{3.2}$$

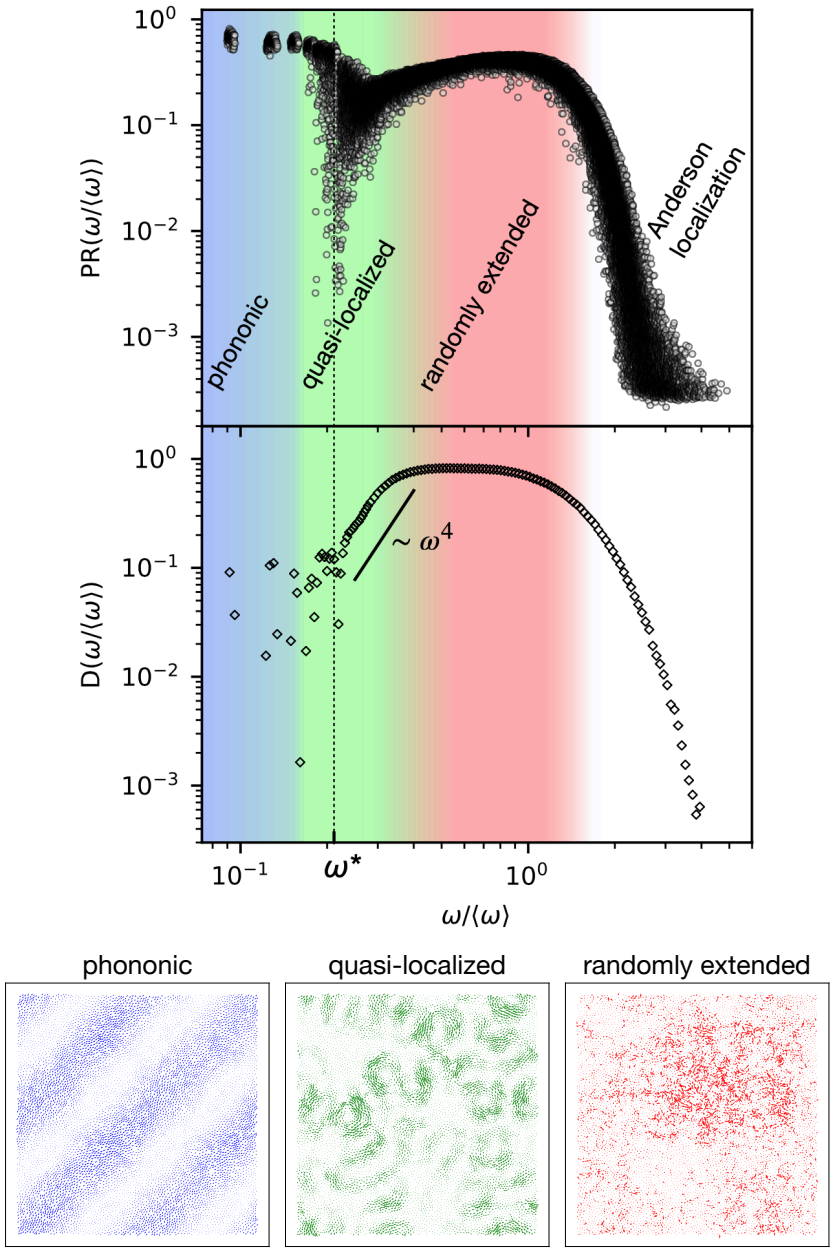

FIGURE 7. Top: participation ratio and vibrational density of states for a packing of $N = 8192$ particles in $d = 3$ at $\Delta\varphi = 3 \times 10^{-2}$. Bottom: real space representation of the eigenvectors for a packing of $N = 8192$ particles in $d = 2$ with distance from jamming $\Delta\varphi = 3 \times 10^{-2}$. Left: phonon with characteristic plane wave modulation. Center: quasi-localized mode with localized excitations distributed over the whole system. Right: extended anomalous mode which correlates a large portion of the system with random excitations.

where N_s is the number of stable particles, i.e. those with at least $z = d + 1$ force bearing neighbors [101]. A mode which corresponds to a totally extensive motion in which every particle participates equally will be characterized by PR $= 1$, whereas a mode completely localized to a single particle will have PR $= 1/N_s$ [1, 62].

The vibrational spectrum for both two and three dimensional packings produced by minimization of the logarithmic potential can be divided into four different ranges of frequency as illustrated in Fig. 7 a, ranging from lowest to highest frequency: 1) At lowest frequencies, the modes separate into discrete phonon bands with PR $\simeq 2/3$ as expected for plane waves [1, 86] (blue region). 2) For frequencies close to ω^* we find quasi-localized modes which show a splitting in the PR and a power-law decay in the density of states (green region). 3) For higher frequencies modes become increasingly delocalized as indicated by a very high PR. This region corresponds to extended anomalous modes as evidenced by a nearly flat density of states (red region). 4) At highest frequencies modes are strongly localized as a result of Anderson localization in a random medium and have a density of states that decays rapidly with increasing frequency [85].

We analyze the diverse nature of the vibrational modes by looking at the real space representation of their eigenvectors shown in Fig. 7 b. Phonons (left) have a typical plane wave modulation which spans the system. Quasi-localized modes (center), with frequencies near ω^*, present a number of localized distortions and vortices hybridized with those phonons at nearby frequencies. Extended anomalous modes (right) contain random seeming excitations spread throughout the entire system.

As shown in Fig. 8 systems in two and three dimensions differ significantly within the quasi-localized frequency range as evidenced both in the PR and the VDOS. Three dimensional have a greater fraction of modes with strong localization than in two dimensional systems. This difference manifests in the functional form of the decay of the VDOS. For $d = 3$ the density of quasi-localized modes dominates over that of extended modes as evidenced by a decay that follows the ω^4 law. For $d = 2$ instead, a continuous crossover between phonons and extended modes dominates this region of the spectrum with a decay of the density that goes as ω^2. These results for hard sphere systems below jamming agree with previous observations for soft spheres above the jamming threshold [1].

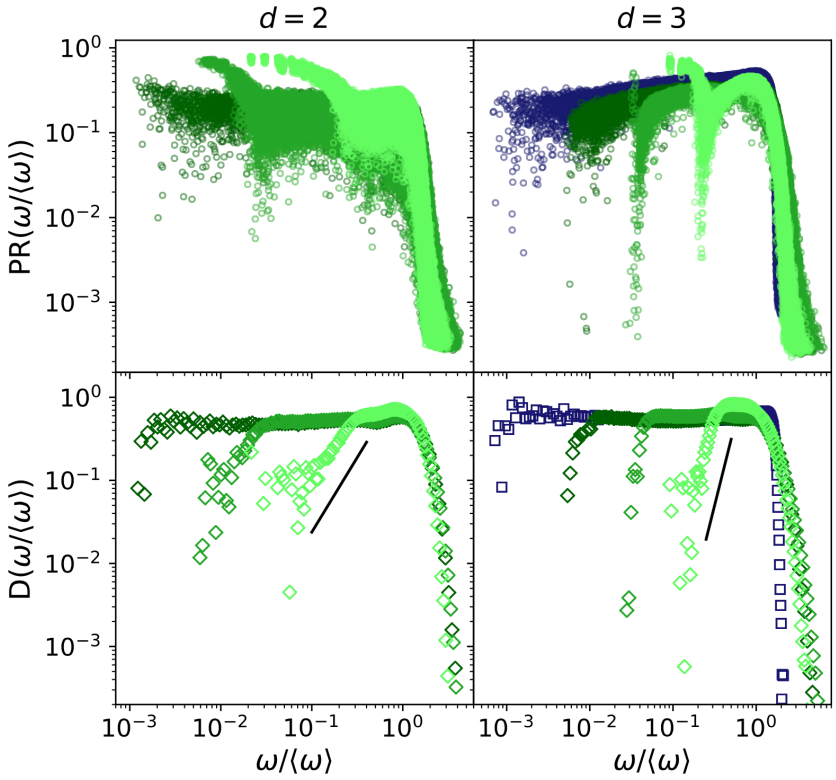

FIGURE 8. Evolution of participation ratio (PR) and vibrational density of states along the compression as a function of $\Delta\varphi$ in $d = 2$ (left) and $d = 3$ (right). Data from compressions are shown in green and that from decompressions in $d = 3$ in blue. Each scatter plot of PR shows data from 10 samples while the density of state curves are averaged over the same number of samples. The distance from jamming increases from left to right. In $d = 3$ $\Delta\varphi = 1.1 \times 10^{-7}$, $\Delta\varphi = 2.3 \times 10^{-5}, 5 \times 10^{-4}, 3 \times 10^{-2}$. In $d = 2$ $\Delta\varphi = 2.7 \times 10^{-6}, 3 \times 10^{-4}, 3 \times 10^{-2}$. The low-frequency decay of the density of states in $d = 2$ follows ω^2 for every value of $\Delta\varphi$ while in $d = 3$ it follows ω^4 sufficiently far from jamming.

Criticality near jamming

Fig. 8 show the evolution of the density of states and the participation ratio for systems in both $d = 2$ and $d = 3$ at a broad range of distances from jamming. As jamming is approached quasi-localized modes move toward lower frequencies and hybridize with the existing phonons as local excitations get softer [87]. For a range of densities sufficiently far from jamming, quasi-localized modes coexist with phonons. For $\Delta\varphi \lesssim 10^{-4}$ extended modes dominate the vibrational spectrum. Localized excitations disappear due to the increasing stability of the packing from the compression, a property which translates into a reduction of the number of soft spots from which

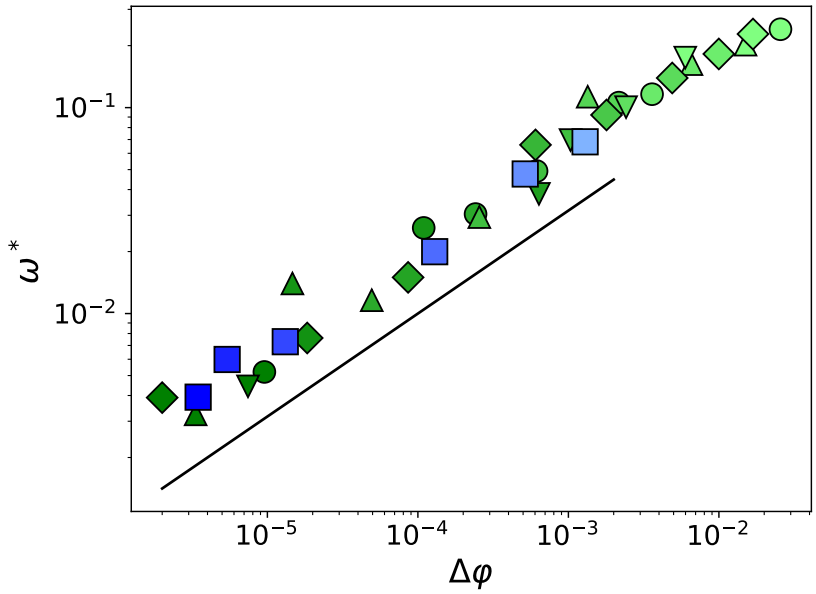

FIGURE 9. Scaling of ω^* as a function of $\Delta\varphi$ for different system sizes from decompressions (blue squares $N = 4096$) and compressions (green circles $N = 1024$, upward triangles $N = 2048$, downward triangles $N = 4096$, diamonds $N = 8192$). Data are consistent with the critical scaling $\omega^* \sim \Delta\varphi^{1/2}$ observed for soft spheres.

localized excitations originate [87]. We observe that for $\Delta\varphi \lesssim 10^{-5}$ localized distortions are suppressed for both spatial dimensions as the extended mode plateau reaches down towards $\omega = 0$. We observe that in $d = 3$ the low frequency scaling of the VDOS deviates from the ω^4 law while in $d = 2$ the ω^2 scaling holds for every step of the compression.

We measure ω^* as the frequency of the last extended mode above a cutoff in participation ratio, $\mathrm{PR_c} = 8 \times 10^{-2}$. As shown in the Supplementary Materials, the results are insensitive to the choice of $\mathrm{PR_c}$ for $8 \times 10^{-2} < \mathrm{PR_c} < 2 \times 10^{-1}$. The relationship of ω^* on $\Delta\varphi$ is reported in Fig. 9. The resulting scaling law is consistent with that already found in the jamming critical region for harmonic soft spheres [75].

Conclusions

By minimizing the logarithmic effective potential we are able to track the structural features from which the mechanical properties of hard sphere glasses originate, both below jamming and at the transition. We have exploited the analytic effective potential to implement

a deterministic minimization algorithm and to compute the vibrational properties of hard sphere glasses, something which previously was accessible only from the velocity autocorrelation function in thermal simulations [57]. The vibrational modes found below and at jamming using this effective potential quantitatively agree with those observed in soft sphere systems above the transition. Thus, we have demonstrated that granular systems and the shadow systems of colloidal glasses have the same vibrational properties at jamming and approaching the transition. Further, the scaling of ω^* confirms that the jamming criticality is universal from both the hard and the soft sides of the transition: thermal hard spheres under very high pressure (or their athermal mapping in this case) have the same criticality as a packing of harmonic soft spheres brought close to zero pressure.

This work suggests several paths forward for studying hard sphere glassy systems using the tools developed for athermal soft sphere systems. First, it would be useful to apply these techniques to develop a more detailed characterization of the size distribution of soft spots in higher dimension, for which existing methods in identifying quasi-localized modes are not sufficient. Further development of real-space characterizations of these modes will allow for investigations of spatial correlations of quasi-localized modes and how the associated lengthscale evolves towards jamming. Another future direction will be to minimize the logarithmic potential in a previously equilibrated hard sphere glass [42]. By doing so, it will be possible to isolate structural features from thermal noise and study mechanical and rheological properties directly related to the real space glassy structure.

Acknowledgements

We thank A. Altieri, C. Brito and S. Franz for useful discussions about the logarithmic potential and L. Berthier, E. Flenner, A. Ikeda and A. Liu for fruitful suggestions. This work was funded by the NSF Career Award grant No. DMR-1255370, and the Simons Collaborations on Cracking the Glass Problem (No. 454939 E. Corwin).

CHAPTER IV

MARGINAL STABILITY ENABLES MEMORY ENCODING IN JAMMED SOLIDS

Introduction

When subject to a repeated driving, amorphous solids are able to adapt their spatial structure to the external deformation [7]. By doing so, they store a memory of the periodic driving as a structural information which can be later extracted [102, 103]. A widely used protocol for encoding a memory in jammed solids is cyclic shear training [7, 104]: the system is repeatedly sheared with cycles of strain amplitude γ_{train}, until it reaches a periodic orbit, i.e. a sequence of rearrangements that the system undergoes every time the same cyclic perturbation is applied. Cyclic shear training finds an explanation in the complex energy landscape of amorphous solids [105, 106] where each rearrangement corresponds to a transition between two energy minima. As the training goes on, the system finds the most energetically favorable path between minima optimizing the mechanical response to the cyclic deformation [104, 107]. While previous studies have shown that cyclic shear brings the system to a lower energy minimum [108], recent advances in producing extremely annealed glassy configurations in thermal [109] and athermal simulations [110] have led to the conclusion that the rheology of amorphous solids is ruled by the preparation protocol [37, 111, 112]. In particular, cyclic shear is only efficient in lowering the energy of marginally stable glasses [108, 112], i.e. configurations that become unstable under very small perturbations [2, 66]. By contrast, cyclic shear fails to further anneal highly stable glassy configurations [112]. Here, we explore the connection between memory training by cyclic shear and mechanical stability in jammed solids and show that memory training is only possible when the system, or a portion of it, is marginally stable.

We produce highly stable packings of jammed soft spheres via a recently developed algorithm based on the simultaneous minimization of positional and radial degrees of freedom [113], while a conventional FIRE minimization is used to produce marginally stable packings [3, 48]. While marginally stable packings show ductile behavior upon increasing the applied shear strain [6], highly stable packings are brittle and yield by forming a shear band [37, 71, 110, 114]. Subject to cyclic shear training, marginally stable packings store memories down to low strain amplitudes and show a uniform participation to the training. By

contrast, highly stable packings can only store memories past the yielding strain and only the particles in the shear band actively participate to the training. Here we show that the shear band is a marginally stable region of the system and its size controls the memory training.

Numerical methods

We produce samples of athermal soft sphere packings using the `pyCudaPacking` package developed by Corwin *et al.* [54, 99]. Each packing is composed of N particles contained in a three dimensional simulation box of unitary volume with periodic boundary conditions. Particles interact via the soft sphere harmonic contact potential

$$U_{ij} = q_{ij}^2 \Theta(q_{ij}) \ , \quad q_{ij} = 1 - \frac{|\vec{r}_{ij}|}{\sigma_{ij}} \tag{4.1}$$

where $\vec{r}_{ij}$ is the distance between particles i and j, σ_{ij} is the sum of their radii, and Θ is the Heaviside step function. We use a log-normal distribution of particle sizes with 20% polydispersity to avoid nucleation of crystalline structures. This model undergoes the jamming transition at zero pressure where particles share just enough contacts to enforce global rigidity [3]. We produce marginally stable packings by minimizing the energy with respect to only positional degrees of freedom via the FIRE algorithm [100]. To produce highly stable packings, we add particle radii as constrained variables to the minimization. In particular, we start from a configuration with random positions and polydisperse size distribution, and allow both particle positions and radii to relax in order to minimize the energy. To keep the initial size distribution fixed, we constrain the radial components of the particle forces by fixing a set of moments of the distribution, namely $\{-6, -3, 3\}$ [113]. Once the energy is minimized, we fix the radii and perform the shear training.

We simulate athermal quasistatic shear (AQS) along the yx direction by applying steps of $\Delta\gamma = 10^{-3}$ strain with Lees-Edwards boundary conditions. A single strain step consists of an affine displacement of each particle $(x_i, y_i, z_i) \to (x_i, y_i + \Delta\gamma x_i, z_i)$, followed by a minimization of the potential energy with respect to the positional degrees of freedom only. We choose to study configurations produced at pressure $P_0 \simeq 0.08$ to optimize the computational cost of our simulations which slows down as the jamming transition is approached.

The rheology of marginally stable and highly stable packings is depicted in Fig. 10. Marginally stable packings show ductile behavior as they encounter the first instability at very

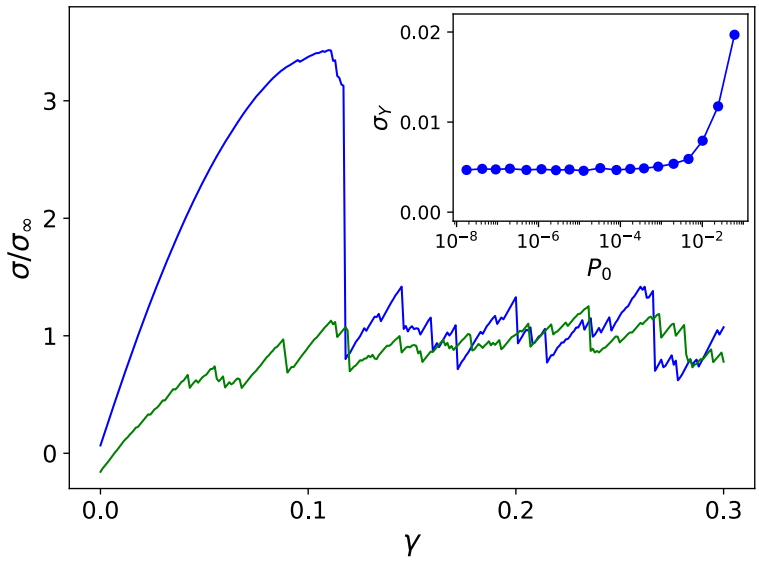

FIGURE 10. Stress vs. strain curves for highly stable (blue) and marginally stable (green) packings produced at pressure $P_0 \simeq 0.08$ and composed of $N = 4096$ particles. The stress is scaled by its typical value σ_∞ in the plastic regime after yielding. Inset: yielding stress, σ_Y, as a function of the initial pressure, P_0, at which brittle packings are produced.

small strain and yield through a series of plastic rearrangements [6]. On the other hand, highly stable packings are brittle: they show an elastic response up to a large yielding strain, γ_Y. After yielding, a sharp stress drop signals the failure under the external load and the system breaks along a shear band [110, 114]. In the inset of Fig. 10, we plot the yielding stress, σ_Y, of highly stable packings as a function of the pressure at which they are produced, P_0. The yielding stress plateaus to a finite value as the jamming point is approached in the limit $P_0 \to 0$ showing that highly stable packings are brittle down to extremely low pressures.

Evolution of stability under shear

To understand the relation between the mechanical stability of a packing and its ability to store memories of shear amplitudes, we first study the evolution of mechanical stability upon increasing the applied shear strain. Before reaching the yielding transition, highly stable packings are characterized by a smooth rise of both pressure and energy in the elastic regime. At the same time, the low-frequency vibrational density of states, which rules the linear response of the system [83], is progressively shifted towards lower frequencies. These properties suggest that

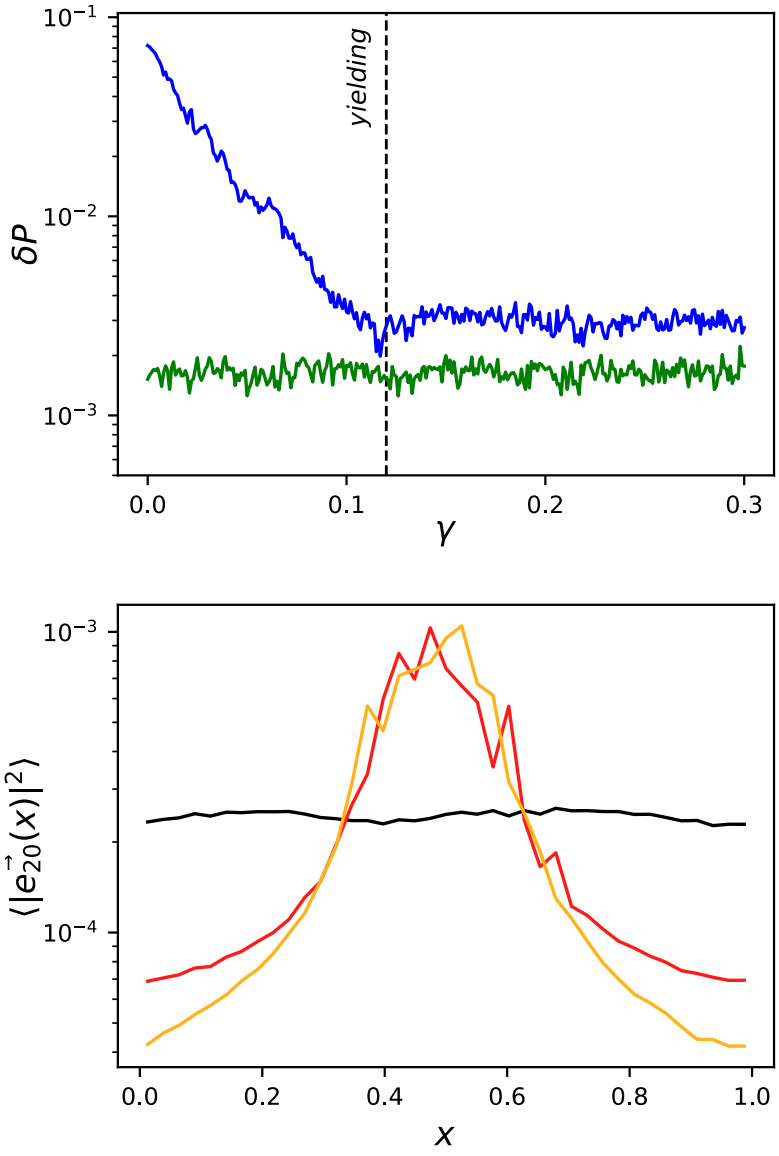

FIGURE 11. Top: pressure change, δP, required to push a packing to a nearby instability as a function of the applied strain γ averaged over 20 samples for both highly stable (blue) and marginally stable (green) packings of $N = 4096$ particles. The dotted line indicates the average yielding strain of highly stable packings. Bottom: magnitudes of the first 20 low-frequency eigenvectors, averaged over slices of the system along the x axis at zero strain (black), right after yielding at $\gamma = 0.122$ (red), and in the plastic regime at $\gamma = 0.3$ (yellow) for a highly stable packing. Data are shifted to center the shear band.

highly stable packings would become unstable under an increasingly smaller perturbation as they approach the yielding point. We investigate how the stability of a packing evolves during AQS by computing the change in pressure, δP, required to push the system to an instability without changing the contact network [113], as reported in the top panel of Fig. 11. In marginally stable packings, the distance to a nearby instability fluctuates around a typical value across all the explored range of strain. Highly stable packings present a very different behavior. At zero strain, they require a large change in pressure to find a nearby instability. As the system is progressively sheared, δP decreases following an exponential decay which ends at the yielding point. After yielding, δP follows a similar behavior as for marginally stable packings. The behavior of δP implies that highly stable packings lose stability and become marginally stable after yielding.

We then explore how the progressive loss of stability in highly stable packings influences the spatial structure of the system by computing the first 20 low-frequency eigenvectors of the Hessian, i.e. the vibrational modes which control the particle motion under small perturbations [83]. In the bottom panel of Fig. 11, we report the averaged magnitude of the low-frequency eigenvectors as a function of the applied strain. At zero strain, the motion due to small perturbations spans the entire system uniformly, a typical behavior for highly stable jammed solids [1]. After yielding, the motion of the low-frequency eigenvectors stays confined in the shear band while the rest of the system is less susceptible to external perturbations. The shear band is then a marginally stable region of the system where particles are more likely to rearrange under quasistatic deformations. We can now show that the existence of a shear band in highly stable packings past yielding is necessary for training a memory by cyclic shear.

Memory training

We use AQS to encode a memory of a strain amplitude, γ_{train}, by cyclic shear in both marginally and highly stable packings. The following results represent averages over 35 samples of $N = 1024$ particles for both cases. We train a packing by repeating shear cycles until the system reaches a periodic orbit which we identify when the energy at the end of a cycle does not change after one or more consecutive cycles. The encoded memory can then be extracted using a readout [8, 102]: starting from a configuration at zero strain, we perform a cycle of strain

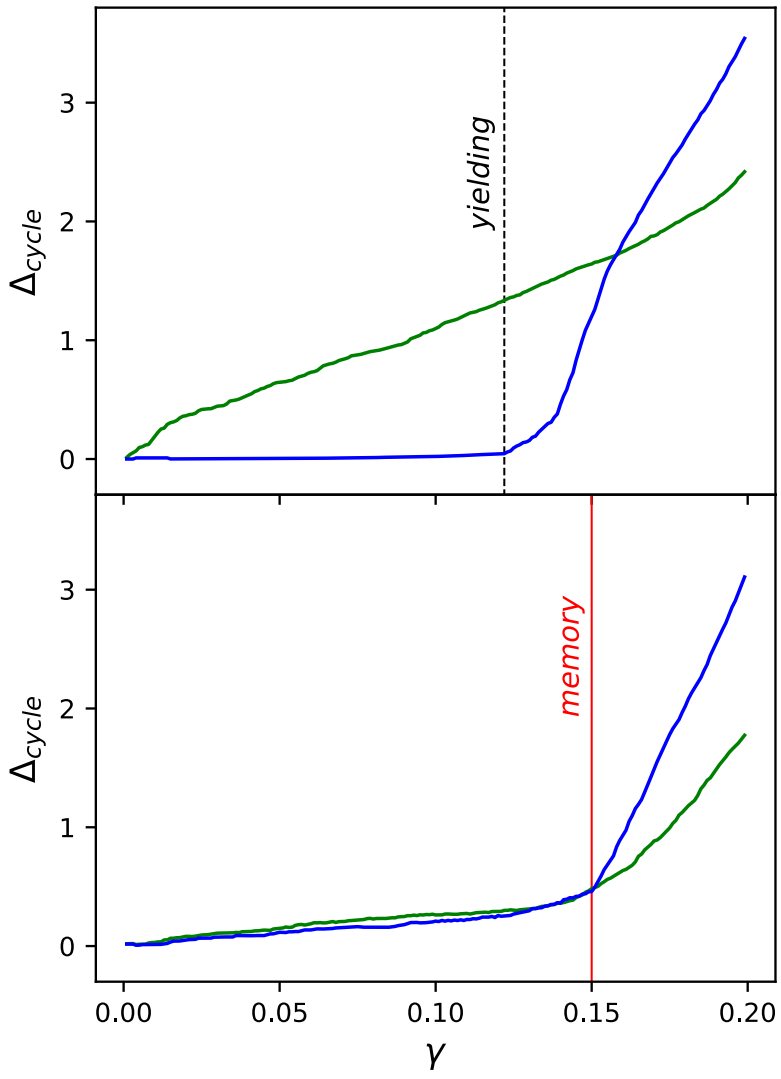

FIGURE 12. Readout shear: Δ_{cycle} as a function of the strain amplitude γ for untrained (top) and trained (bottom) configurations of highly stable (blue) and marginally stable (green) packings. The solid red line indicates the encoded strain amplitude, $\gamma_{train} = 0.15$, and the dashed black line shows the average yielding strain for highly stable packings.

amplitude γ and measure the distance between the initial and final configurations as

$$\Delta_{cycle} = \sqrt{\sum_i |\vec{r}_i^{\,final} - \vec{r}_i^{\,initial}|^2} \quad , \tag{4.2}$$

where the sum runs over the stable particles, i.e. those with at least $d + 1$ force bearing contacts [101]. The readout is performed for a range of strain amplitudes $\gamma \in [0, 0.2]$, separated by an increment of $\Delta\gamma = 10^{-3}$.

Before training a memory, the readout plots for marginally and highly stable packings show two very different behaviors, as can be seen from the top panel of Fig. 12. The readout for highly stable packings (blue) shows that these are reversible for any cycles with $\gamma < \gamma_Y$ as Δ_{cycle} stays equal to zero up to the yielding transition. After the brittle failure, Δ_{cycle} shows an upturn and the system becomes irreversible. For marginally stable packings (green), by contrast, Δ_{cycle} monotonically increases from zero starting at the beginning of the readout. This indicates that a marginally stable packing undergoes irreversible rearrangements for all the explored strain amplitudes. The readout plots for trained packings is shown in the bottom panel of Fig. 12. Here, Δ_{cycle} stays close to zero for cycles of strain amplitudes smaller than the training strain, $\gamma_{train} = 0.15$. Note that γ_{train} is larger than the average yielding strain of highly stable packings. For $\gamma > \gamma_{train}$, both plots show a quick upturn, which is a signature of the memory encoded by cyclic shear training.

We study the trainability of our packings by plotting the number of training cycles, N_{cycles}, needed to encode a memory as a function of the training strain amplitude, γ_{train}, see Fig. 13. While marginally stable packings store memories for all the explored ranges of γ_{train}, highly stable packings are able to store memories only for strain amplitudes larger than the yielding strain. Moreover, at a fixed strain amplitude, highly stable packings need a larger N_{cycles} to reach a periodic orbit compared to marginally stable packings. This is due to the difference in the fraction of particles which are actively participating to the training: while in marginally stable packings all the particles are uniformly displaced by the shear cycles, in highly stable packings the particles within the shear band rearrange much more than others.

To support this claim, we study the relation between marginal stability and the number of training cycles by tuning the width of the shear band. This is accomplished by shearing brittle packings with an initial cycle of large strain amplitude, γ_{break}, before performing cyclic

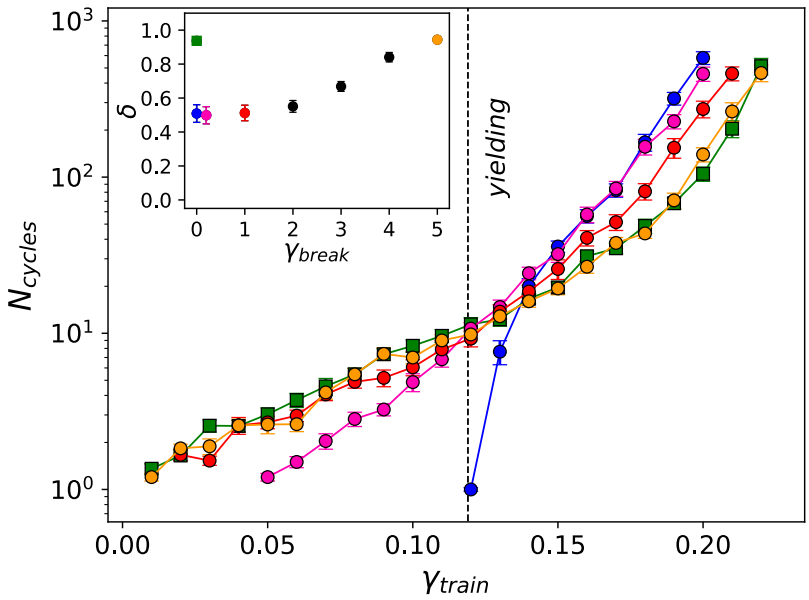

FIGURE 13. Number of training cycles required to encode a memory, N_{cycles}, as a function of the encoded strain amplitude γ_{train} for brittle (blue) and ductile (green) packings as well as brittle packings that are broken with a single cycle of strain amplitude of $\gamma_{break} = 0.2$ (pink), 1 (red) and 5 (yellow) before the training. Inset: shear band size, δ, as a function of γ_{break} after training a memory of $\gamma_{train} = 0.15$ with the same color code as in the main plot. The error bars represent the standard error on the mean.

shear training at a given γ_{train}. During the breaking cycle, particles adjacent to the shear band relax and lose their initial stability. We estimate the size of the shear band, δ, by computing the distribution of Δ_{cycle} along one of the transverse directions to shear and extracting the width of the distribution peak. We measure δ after both the initial breaking cycle and cyclic shear training and find it to be the same within error. As shown in the inset of Fig. 13, the size of the shear band computed after training a memory of $\gamma_{train} = 0.15$ is proportional to γ_{break}. Fig. 13 shows that for any γ_{break}, broken brittle packings are able to store memories of strain amplitudes below the yielding strain. As γ_{break} increases, the trainability curve gets closer to the one for ductile packings (green). For $\gamma_{break} = 5$ (yellow), the shear band is spread out to the entire system and the number of training cycles for strain amplitudes above the yielding strain are similar to those reported for ductile packings. As the shear band broadens, more particles actively participate to the training. The existence of a shear band is thereby necessary to store a memory by cyclic shear

in brittle packings, suggesting that memories can only be formed in marginally stable regions of the system.

Conclusions

In this Letter, we explore the role of mechanical stability in the context of memory training by cyclic shear in jammed solids. While marginally stable packings are able to store memories for all the explored strain amplitudes, we observe that highly stable packings need to first overcome brittle yielding and form a shear band in order to do so. Here is where mechanical stability comes into play: brittle packings become marginally stable after yielding and marginal stability is confined in the shear band where most of the rearrangements during the training take place. This result shows that memory training in jammed packings is only possible if the system, or a portion of it, is marginally stable.

The strong connection between memory training and mechanical stability suggests that the development of memory in real space is coupled to the evolution of the low-frequency vibrational modes, an aspect of memory training which requires further investigation. An exciting new direction would be to extend the work conducted here to soft sphere packings driven by athermal quasi-static random displacements, an active matter model introduced in theory [115] and simulations [116], where the brittle failure happens in regions randomly distributed across the system. Training a highly stable packing with this new cyclic driving could potentially allow for encoding memories in pockets of the system which could be preemptively designed, broadening the application scope of trainable jammed solids.

Acknowledgements

We thank Ian Graham, Peter Morse, Sidney Nagel and Sri Sastry for fruitful discussions on memory formation. This work was funded by the NSF Career Award grant No. DMR-1255370, and the Simons Collaboration on Cracking the Glass Problem (No. 454939 E. Corwin).

CHAPTER V

SUPPLEMENTAL MATERIALS FOR CHAPTER 2

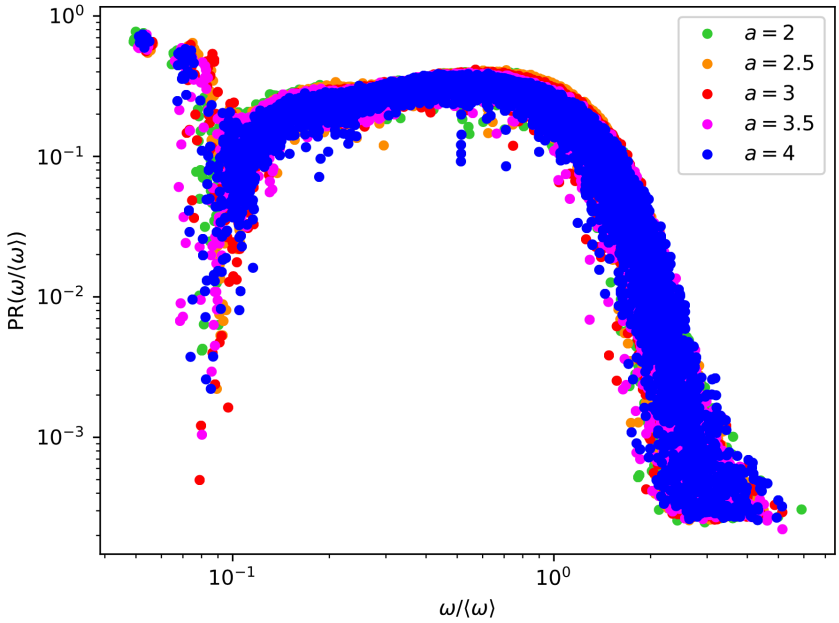

FIGURE 14. Participation ratio (PR) as a function of the gap distance cutoff h_{cut} for the logarithmic potential for a typical sample. Curves are plotted for $h_{cut} = ah_{peak}$ with a ranging from 2 to 4, where h_{peak} is the size of the gap at the first peak of the gap distribution. Samples are obtained by compressing the same initial packing of $N = 8192$ particles in $d = 3$ from a starting packing fraction of $\varphi = 0.55$. Data are plotted for $\varphi = 0.65722$. The PR does not show any significant difference as the cutoff distance changes over the full frequency range.

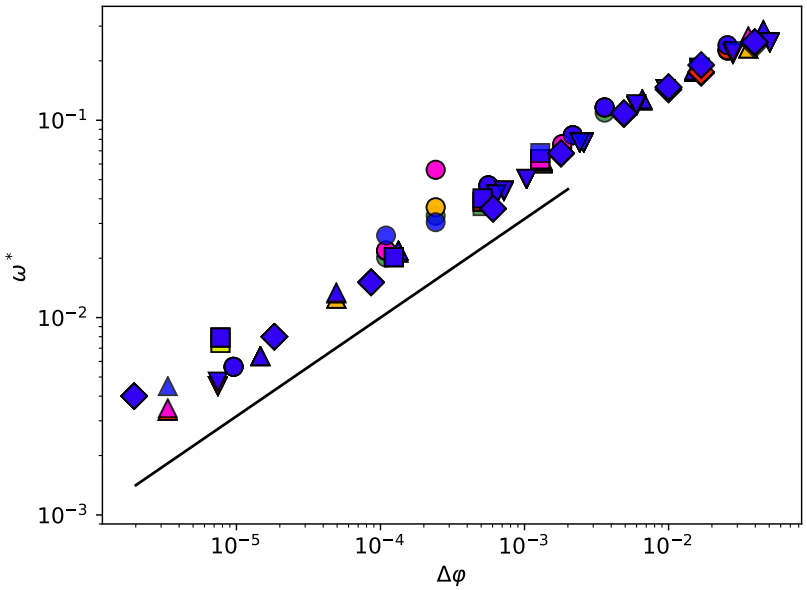

FIGURE 15. Dependence of ω^* on $\mathrm{PR_c}$, the cutoff threshold for the participation ratio, $\mathrm{PR_c} = 0.2$ (green), 0.18 (yellow), 0.15 (orange), 0.12 (red), 0.1 (magenta), 0.08 (blue). The curves are plotted for different system sizes from decompressions (squares $N = 4096$) and compressions (circles $N = 1024$, upward triangles $N = 2048$, downward triangles $N = 4096$, diamonds $N = 8192$). The scaling relation between ω^* and $\Delta\varphi$ is not affected by the choice of $\mathrm{PR_c}$ for $8 \times 10^{-2} < \mathrm{PR_c} < 2 \times 10^{-1}$, values which correspond to 8% and 20% participating particles respectively.

CHAPTER VI

CONCLUSION

The work presented in this dissertation clarifies how the amorphous structure of jammed solids influences the vibrational and mechanical properties of the system. Here, the mechanical response of jammed packings of hard and soft sphere packings has been investigated under either compression or shear deformation in the limit of zero temperature where both systems experience rigidity. Two main results have been discussed. First, the critical behavior of thermal hard sphere glasses and granular soft sphere packings merge at the jamming transition, where these two models share the same vibrational properties. Second, the mechanical stability of the amorphous structure controls the rheology of jammed solids and their ability to adapt to a cyclic shear driving. These results answer questions on the nature of the mechanical response of amorphous solids as well as opening up new avenues of research in different fields.

Chapter II encompasses the latest theoretical advances on the glass transition and the amorphous solid phase from an infinite-dimensional perspective. In the first part of the chapter, the physics of glasses is explored by using a state-following algorithm on a system of thermal hard spheres, a framework which allows one to build the glassy phase diagram by controlling the temperature and density of the system. Starting from a liquid configuration at equilibrium, the system is rapidly cooled or compressed until it undergoes a dynamical arrest at the glass transition. Upon further compression or cooling, the dynamics of the system becomes even slower and the system gets stuck in a marginally stable configuration. In the limit of zero temperature or infinite pressure a marginally stable glass jams and thermal fluctuations are no longer relevant to describe the physical properties of the system. Although this chapter presents a mean field description of glassy physics, the free energy landscape picture reported here offers a powerful tool for interpreting the physical properties of glasses at finite dimensions. In particular, each glassy configuration corresponds to a free energy basin and the system can travel between basins thanks to thermal fluctuations. When the thermal energy is lowered, the system can access a more limited portion of the phase space and the rugged and hierarchical organization of the free energy landscape controls the extremely slow dynamics of the system. At zero temperature, glasses find a unifying point with granular materials as they jam under an infinitely high pressure. The system

can now travel among energy minima only through mechanical deformations and a similar state-following framework can used to explore the energy landscape as a function of applied shear strain and density.

The theory of the amorphous solid phase is presented in the second part of chapter II. The critical properties of soft sphere packings near the jamming point are described, with particular emphasis on the critical scaling of the elastic moduli near the transition. The mechanical and thermal response of amorphous solids is analyzed through the free energy landscape picture which again offers an interpretation of the anomalous behavior with respect to the crystalline counterpart. In particular, the excess of low-frequency vibrational modes is linked to the presence of many marginally stable free energy minima or energy minima at zero temperature. This gives rise to a different scaling of the low-frequency tail of the vibrational density of states which controls the mechanical and thermal properties of the system.

In chapter III, I show that the vibrational properties of thermal hard sphere glasses and soft sphere packings meet at the jamming point. In more detail, as a hard sphere system approaches jamming from below and a soft sphere packings from above, the low-frequency modes computed from samples of both systems give rise the same statistics of the low-frequency tail of vibrational density of states. This enforces that the mechanical properties of hard and soft sphere configurations are uniquely determined by their amorphous structure. In this work I developed a protocol to produce stable configurations of hard spheres right below the jamming point via athermal simulations, a particularly challenging task due to the non-analytical repulsive potential between particles. To overcome this difficulty, I implemented the energy minimization algorithm of an effective potential between hard spheres which is a good approximation of the interaction between frequently colliding particles under very high pressure. The analytical effective potential allowed me to compute the mechanical properties of the system, such as the normal modes and the vibrational density of states, using tools already developed for soft potentials. This work takes a big step forward in linking the properties of granular materials to those of glass-former liquids approaching the rigidity transition.

The technique I developed to produce equilibrated hard spheres configurations has already been used by others in the glass community. It allows one to probe the vibrational properties of thermal hard sphere glasses with a simple and reproducible athermal algorithm, rather than

using conventional thermal simulations which can only give an indirect measure of the vibrational density of states. A future research direction is applying the logarithmic potential minimization on configurations of previously thermalized hard spheres. This would allow to decouple the amorphous structure from the thermal noise and investigate the inherent mechanical properties of the systems. This work also underlines that low-frequency modes, responsible for the linear response of the system, originate from localized weak, often called soft spots. The soft spots distribution has been greatly studied from the soft sphere perspective as it offers a prediction on where structural rearrangements and plastic events would happen. It is now possible to perform similar studies for thermal glasses for which the typical length scale of soft spots have been theorized as a critical correlation length for the jamming transition. This could potentially offer insights for building a finite-dimensional continuum theory of amorphous solids.

In chapter IV, I explore the role of mechanical stability on the rheology of jammed solids. Precisely, I show that cyclic shear driving can be used to encode a memory of a shear deformation only in marginally stable regions of the system. Jammed solids are produced via two protocols which allow to access marginally stable and highly stable configurations of soft spheres interacting via a harmonic contact potential. While the first protocol is based on using a conventional energy minimization, the latter is a recently developed algorithm which introduces the radial degrees of freedom in the minimization of the potential energy. Having access to a richer number of degrees of freedom allows the system to find a better configuration which is highly stable against mechanical deformations. Upon athermal quasistatic shear, marginally stable packings show a ductile behavior whereas highly stable packings have a large elastic response and eventually fail to support the external load at a large yielding strain. When it comes to memory training by cyclic shear, packings produced with a very high mechanical stability are not able to store a memory of strain amplitudes below the yielding strain. The reason is the lack of marginal stability before yielding: highly stable packings are reversible under shear cycles in the elastic regime and cyclic deformations do not change the structure of the system. By contrast, marginally stable packings undergo irreversible rearrangements even for small strain amplitudes as they travel between energy minima which are connected by small perturbations. I show that the ability to access marginally stable configurations during the cyclic shear training is necessary to store a memory. In particular, highly stable packings beyond the yielding point are able to store memories because

they form a shear band, a region of the system which I show to be marginally stable. This work sheds light on the mechanisms responsible for memory formation by mechanical training in jammed solids in relation to the mechanical stability of the system.

In addiction to presenting a quantitative study of memory training by cyclic shear, this work reveals that the development of memory is strongly tied with the amorphous structure of the system. As athermal quasistatic shear has been used to explore the energy landscape of amorphous solids, it can also be used to investigate whether the structural rearrangements during the training influence the normal modes of the system. This could shed light on how the optimization of the structure to the shear deformation is linked to the optimization of the energy landscape in phase space, and potentially clarify whether memory develops as a collective phenomenon arising from localized weak regions, or more as a sequence of avalanches which spans throughout the entire system.

The result presented in chapter IV opens up new directions in the field of memory training in jammed solids. In a preliminary study I observed that multiple memories can be encoded by using shear training on orthogonal shear directions, a phenomenon also observed in experiments of colloidal systems. Along the same lines, I'm currently working on implementing memory training using a newly developed algorithm to simulate the physics of active soft particles: athermal quasistatic random displacements (AQRD). Here, particle activity is schematized as a propulsion in a direction extracted from a random distribution. The rheology of highly stable packings under AQRD has already been explored and a similar brittle behavior has been observed as in the case of simple shear. Nevertheless, a highly stable packing subject to AQRD does not form a shear band upon yielding but the brittle failure originates from localized weak regions of the system. If these regions reveal to be marginally stable as in the case of the shear band in simple shear, memories by cyclic driving of AQRD could potentially develop in localized portions of the system. This would allow to preemptively designed the location where memory gets stored. In particular, recent works on simple shear showed that it is possible to tune the location of the shear band of a brittle amorphous packing by exciting a localized region of the system, producing a weak spot from which the brittle failure originates. In a similar fashion, weak spots could trigger memory to form in determined regions of a packing subjected to cyclic AQRD, a possibility which would represent an important advance in the field of designing materials with particular tasks.

REFERENCES CITED

[1] Hideyuki Mizuno, Hayato Shiba, and Atsushi Ikeda. Continuum limit of the vibrational properties of amorphous solids. *Proceedings of the National Academy of Sciences*, 114(46): E9767–E9774, November 2017. ISSN 0027-8424, 1091-6490. doi: 10.1073/pnas.1709015114. URL http://www.pnas.org/lookup/doi/10.1073/pnas.1709015114.

[2] Patrick Charbonneau, Jorge Kurchan, Giorgio Parisi, Pierfrancesco Urbani, and Francesco Zamponi. Glass and Jamming Transitions: From Exact Results to Finite-Dimensional Descriptions. *Annual Review of Condensed Matter Physics*, 8(1):265–288, 2017. doi: 10.1146/annurev-conmatphys-031016-025334. URL https://doi.org/10.1146/annurev-conmatphys-031016-025334.

[3] Corey S. O'Hern, Leonardo E. Silbert, Andrea J. Liu, and Sidney R. Nagel. Jamming at zero temperature and zero applied stress: The epitome of disorder. *Phys. Rev. E*, 68(1):011306, July 2003. doi: 10.1103/PhysRevE.68.011306. URL https://link.aps.org/doi/10.1103/PhysRevE.68.011306.

[4] Aleksandar Donev, Salvatore Torquato, and Frank H. Stillinger. Pair correlation function characteristics of nearly jammed disordered and ordered hard-sphere packings. *Phys. Rev. E*, 71(1):011105, January 2005. ISSN 1539-3755, 1550-2376. doi: 10.1103/PhysRevE.71.011105. URL https://link.aps.org/doi/10.1103/PhysRevE.71.011105.

[5] Aleksandar Donev, Salvatore Torquato, Frank H. Stillinger, and Robert Connelly. Jamming in hard sphere and disk packings. *Journal of Applied Physics*, 95(3):989–999, February 2004. ISSN 0021-8979, 1089-7550. doi: 10.1063/1.1633647. URL http://aip.scitation.org/doi/10.1063/1.1633647.

[6] Craig E. Maloney and Anaël Lemaître. Amorphous systems in athermal, quasistatic shear. *Phys. Rev. E*, 74(1):016118, July 2006. doi: 10.1103/PhysRevE.74.016118. URL https://link.aps.org/doi/10.1103/PhysRevE.74.016118.

[7] Laurent Corté, P. M. Chaikin, J. P. Gollub, and D. J. Pine. Random organization in periodically driven systems. *Nature Physics*, 4(5):420–424, May 2008. ISSN 1745-2481. doi: 10.1038/nphys891. URL https://www.nature.com/articles/nphys891. Number: 5 Publisher: Nature Publishing Group.

[8] Nathan C. Keim and Sidney R. Nagel. Generic Transient Memory Formation in Disordered Systems with Noise. *Physical Review Letters*, 107(1), June 2011. ISSN 0031-9007, 1079-7114. doi: 10.1103/PhysRevLett.107.010603. URL https://link.aps.org/doi/10.1103/PhysRevLett.107.010603.

[9] Francesco Arceri, François P. Landes, Ludovic Berthier, and Giulio Biroli. Glasses and aging: A Statistical Mechanics Perspective. *arXiv:2006.09725 [cond-mat]*, October 2020. URL http://arxiv.org/abs/2006.09725. arXiv: 2006.09725.

[10] Francesco Arceri and Eric I. Corwin. Vibrational Properties of Hard and Soft Spheres Are Unified at Jamming. *Phys. Rev. Lett.*, 124(23):238002, June 2020. ISSN 0031-9007, 1079-7114. doi: 10.1103/PhysRevLett.124.238002. URL https://link.aps.org/doi/10.1103/PhysRevLett.124.238002.

[11] Gerold Adam and Julian H. Gibbs. On the Temperature Dependence of Cooperative Relaxation Properties in Glass-Forming Liquids. *The Journal of Chemical Physics*, 43(1): 139–146, July 1965. ISSN 0021-9606, 1089-7690. doi: 10.1063/1.1696442. URL http://aip.scitation.org/doi/10.1063/1.1696442.

[12] Wolfgang Götze. Recent tests of the mode-coupling theory for glassy dynamics. *J. Phys.: Condens. Matter*, 11(10A):A1–A45, March 1999. ISSN 0953-8984, 1361-648X. doi: 10.1088/0953-8984/11/10A/002. URL https://iopscience.iop.org/article/10.1088/0953-8984/11/10A/002.

[13] Marc Mezard, Giorgio Parisi, and Miguel Angel Virasoro. *Spin Glass Theory And Beyond: An Introduction To The Replica Method And Its Applications*. World Scientific Publishing Company, November 1987. ISBN 978-981-310-391-7. Google-Books-ID: DwY8DQAAQBAJ.

[14] T. R. Kirkpatrick and D. Thirumalai. Dynamics of the Structural Glass Transition and the p -Spin—Interaction Spin-Glass Model. *Phys. Rev. Lett.*, 58(20):2091–2094, May 1987. ISSN 0031-9007. doi: 10.1103/PhysRevLett.58.2091. URL https://link.aps.org/doi/10.1103/PhysRevLett.58.2091.

[15] T. R. Kirkpatrick and P. G. Wolynes. Connections between some kinetic and equilibrium theories of the glass transition. *Phys. Rev. A*, 35(7):3072–3080, April 1987. ISSN 0556-2791. doi: 10.1103/PhysRevA.35.3072. URL https://link.aps.org/doi/10.1103/PhysRevA.35.3072.

[16] Giulio Biroli and Marc Mézard. Lattice Glass Models. *Phys. Rev. Lett.*, 88(2):025501, December 2001. ISSN 0031-9007, 1079-7114. doi: 10.1103/PhysRevLett.88.025501. URL https://link.aps.org/doi/10.1103/PhysRevLett.88.025501.

[17] David R. Nelson. *Defects and Geometry in Condensed Matter Physics*. Cambridge University Press, March 2002. ISBN 978-0-521-00400-8. Google-Books-ID: YtYFAqswRzUC.

[18] Richard K. Darst, David R. Reichman, and Giulio Biroli. Dynamical heterogeneity in lattice glass models. *The Journal of Chemical Physics*, 132(4):044510, January 2010. ISSN 0021-9606, 1089-7690. doi: 10.1063/1.3298877. URL http://aip.scitation.org/doi/10.1063/1.3298877.

[19] Alejandro Seif and Tomas S. Grigera. Structure and dynamics of the t154 lattice glass. *arXiv:1611.06754 [cond-mat]*, November 2016. URL http://arxiv.org/abs/1611.06754. arXiv: 1611.06754.

[20] Yoshihiko Nishikawa and Koji Hukushima. Lattice Glass Model in Three Spatial Dimensions. *Phys. Rev. Lett.*, 125(6):065501, August 2020. ISSN 0031-9007, 1079-7114. doi: 10.1103/PhysRevLett.125.065501. URL https://link.aps.org/doi/10.1103/PhysRevLett.125.065501.

[21] Gavin D. McCullagh, Davide Cellai, Aonghus Lawlor, and Kenneth A. Dawson. Finite-energy extension of a lattice glass model. *Phys. Rev. E*, 71(3):030102, March 2005. ISSN 1539-3755, 1550-2376. doi: 10.1103/PhysRevE.71.030102. URL https://link.aps.org/doi/10.1103/PhysRevE.71.030102.

[22] O. Rivoire, G. Biroli, O. C. Martin, and M. Mezard. Glass models on Bethe lattices. *The European Physical Journal B - Condensed Matter*, 37(1):55–78, January 2003. ISSN 1434-6028, 1434-6036. doi: 10.1140/epjb/e2004-00030-4. URL http://link.springer.com/10.1140/epjb/e2004-00030-4.

[23] D. J. Gross and M. Mezard. The simplest spin glass. *Nuclear Physics B*, 240(4):431–452, November 1984. ISSN 0550-3213. doi: 10.1016/0550-3213(84)90237-2. URL https://www.sciencedirect.com/science/article/pii/0550321384902372.

[24] Tommaso Castellani and Andrea Cavagna. Spin-glass theory for pedestrians. *J. Stat. Mech.*, 2005(05):P05012, May 2005. ISSN 1742-5468. doi: 10.1088/1742-5468/2005/05/P05012. URL https://iopscience.iop.org/article/10.1088/1742-5468/2005/05/P05012.

[25] Andrea Cavagna. Supercooled liquids for pedestrians. *Physics Reports*, 476(4):51–124, June 2009. ISSN 0370-1573. doi: 10.1016/j.physrep.2009.03.003. URL https://www.sciencedirect.com/science/article/pii/S0370157309001112.

[26] Jorge Kurchan, Giorgio Parisi, and Francesco Zamponi. Exact theory of dense amorphous hard spheres in high dimension I. The free energy. *J. Stat. Mech.*, 2012(10):P10012, October 2012. ISSN 1742-5468. doi: 10.1088/1742-5468/2012/10/P10012. URL https://iopscience.iop.org/article/10.1088/1742-5468/2012/10/P10012.

[27] Jorge Kurchan, Giorgio Parisi, Pierfrancesco Urbani, and Francesco Zamponi. Exact Theory of Dense Amorphous Hard Spheres in High Dimension. II. The High Density Regime and the Gardner Transition. *J. Phys. Chem. B*, 117(42):12979–12994, October 2013. ISSN 1520-6106, 1520-5207. doi: 10.1021/jp402235d. URL https://pubs.acs.org/doi/10.1021/jp402235d.

[28] Giorgio Parisi, Pierfrancesco Urbani, and Francesco Zamponi. *Theory of Simple Glasses: Exact Solutions in Infinite Dimensions*. Cambridge University Press, January 2020. ISBN 978-1-108-12610-6. Google-Books-ID: NZ7MDwAAQBAJ.

[29] Monica Skoge, Aleksandar Donev, Frank H. Stillinger, and Salvatore Torquato. Packing hyperspheres in high-dimensional Euclidean spaces. *Phys. Rev. E*, 74(4):041127, October 2006. ISSN 1539-3755, 1550-2376. doi: 10.1103/PhysRevE.74.041127. URL https://link.aps.org/doi/10.1103/PhysRevE.74.041127.

[30] J. A. van Meel, B. Charbonneau, A. Fortini, and P. Charbonneau. Hard-sphere crystallization gets rarer with increasing dimension. *Phys. Rev. E*, 80(6):061110, December 2009. ISSN 1539-3755, 1550-2376. doi: 10.1103/PhysRevE.80.061110. URL https://link.aps.org/doi/10.1103/PhysRevE.80.061110.

[31] Patrick Charbonneau, Jorge Kurchan, Giorgio Parisi, Pierfrancesco Urbani, and Francesco Zamponi. Exact theory of dense amorphous hard spheres in high dimension. III. The full replica symmetry breaking solution. *Journal of Statistical Mechanics: Theory and Experiment*, 2014(10):P10009, October 2014. ISSN 1742-5468. doi: 10.1088/1742-5468/2014/10/P10009. URL http://stacks.iop.org/1742-5468/2014/i=10/a=P10009?key=crossref.93ca485b5c8a929d2fce0ccc59863568.

[32] Camille Scalliet, Ludovic Berthier, and Francesco Zamponi. Marginally stable phases in mean-field structural glasses. *Phys. Rev. E*, 99(1):012107, January 2019. doi: 10.1103/PhysRevE.99.012107. URL https://link.aps.org/doi/10.1103/PhysRevE.99.012107. Publisher: American Physical Society.

[33] Giorgio Parisi and František Slanina. Toy model for the mean-field theory of hard-sphere liquids. *Phys. Rev. E*, 62(5):6554–6559, November 2000. ISSN 1063-651X, 1095-3787. doi: 10.1103/PhysRevE.62.6554. URL https://link.aps.org/doi/10.1103/PhysRevE.62.6554.

[34] Giorgio Parisi and Francesco Zamponi. Mean-field theory of hard sphere glasses and jamming. *Rev. Mod. Phys.*, 82(1):789–845, March 2010. doi: 10.1103/RevModPhys.82.789. URL https://link.aps.org/doi/10.1103/RevModPhys.82.789.

[35] E. Gardner. Spin glasses with p-spin interactions. *Nuclear Physics B*, 257:747–765, January 1985. ISSN 0550-3213. doi: 10.1016/0550-3213(85)90374-8. URL https://www.sciencedirect.com/science/article/pii/0550321385903748.

[36] Ludovic Berthier, Giulio Biroli, Patrick Charbonneau, Eric I. Corwin, Silvio Franz, and Francesco Zamponi. Gardner physics in amorphous solids and beyond. *J. Chem. Phys.*, 151 (1):010901, July 2019. ISSN 0021-9606, 1089-7690. doi: 10.1063/1.5097175. URL http://aip.scitation.org/doi/10.1063/1.5097175.

[37] Corrado Rainone and Pierfrancesco Urbani. Following the evolution of glassy states under external perturbations: the full replica symmetry breaking solution. *J. Stat. Mech.*, 2016 (5):053302, May 2016. ISSN 1742-5468. doi: 10.1088/1742-5468/2016/05/053302. URL https://iopscience.iop.org/article/10.1088/1742-5468/2016/05/053302.

[38] Silvio Franz, Giorgio Parisi, Maxime Sevelev, Pierfrancesco Urbani, and Francesco Zamponi. Universality of the SAT-UNSAT (jamming) threshold in non-convex continuous constraint satisfaction problems. *SciPost Phys.*, 2(3):019, June 2017. ISSN 2542-4653. doi: 10.21468/SciPostPhys.2.3.019. URL https://scipost.org/10.21468/SciPostPhys.2.3.019.

[39] Camille Scalliet and Ludovic Berthier. Rejuvenation and Memory Effects in a Structural Glass. *Phys. Rev. Lett.*, 122(25):255502, June 2019. doi: 10.1103/PhysRevLett.122.255502. URL https://link.aps.org/doi/10.1103/PhysRevLett.122.255502. Publisher: American Physical Society.

[40] Qinyi Liao and Ludovic Berthier. Hierarchical Landscape of Hard Disk Glasses. *Phys. Rev. X*, 9(1):011049, March 2019. ISSN 2160-3308. doi: 10.1103/PhysRevX.9.011049. URL https://link.aps.org/doi/10.1103/PhysRevX.9.011049.

[41] Camille Scalliet, Ludovic Berthier, and Francesco Zamponi. Nature of excitations and defects in structural glasses. *Nature Communications*, 10(1):5102, November 2019. ISSN 2041-1723. doi: 10.1038/s41467-019-13010-x. URL https://www.nature.com/articles/s41467-019-13010-x. Number: 1 Publisher: Nature Publishing Group.

[42] Ludovic Berthier, Patrick Charbonneau, Yuliang Jin, Giorgio Parisi, Beatriz Seoane, and Francesco Zamponi. Growing timescales and lengthscales characterizing vibrations of amorphous solids. *Proc Natl Acad Sci U S A*, 113(30):8397–8401, July 2016. ISSN 0027-8424. doi: 10.1073/pnas.1607730113. URL https://www.ncbi.nlm.nih.gov/pmc/articles/PMC4968735/.

[43] Camille Scalliet, Ludovic Berthier, and Francesco Zamponi. Absence of Marginal Stability in a Structural Glass. *Phys. Rev. Lett.*, 119(20):205501, November 2017. ISSN 0031-9007, 1079-7114. doi: 10.1103/PhysRevLett.119.205501. URL https://link.aps.org/doi/10.1103/PhysRevLett.119.205501.

[44] Thibaud Maimbourg, Jorge Kurchan, and Francesco Zamponi. Solution of the Dynamics of Liquids in the Large-Dimensional Limit. *Phys. Rev. Lett.*, 116(1):015902, January 2016. ISSN 0031-9007, 1079-7114. doi: 10.1103/PhysRevLett.116.015902. URL https://link.aps.org/doi/10.1103/PhysRevLett.116.015902.

[45] Pinaki Chaudhuri, Ludovic Berthier, and Srikanth Sastry. Jamming Transitions in Amorphous Packings of Frictionless Spheres Occur over a Continuous Range of Volume Fractions. *Phys. Rev. Lett.*, 104(16):165701, April 2010. ISSN 0031-9007, 1079-7114. doi: 10.1103/PhysRevLett.104.165701. URL https://link.aps.org/doi/10.1103/PhysRevLett.104.165701.

[46] Andrea J. Liu and Sidney R. Nagel. The Jamming Transition and the Marginally Jammed Solid. *Annual Review of Condensed Matter Physics*, 1(1):347–369, 2010. doi: 10.1146/annurev-conmatphys-070909-104045. URL https://doi.org/10.1146/annurev-conmatphys-070909-104045. _eprint: https://doi.org/10.1146/annurev-conmatphys-070909-104045.

[47] Corey S. O'Hern, Stephen A. Langer, Andrea J. Liu, and Sidney R. Nagel. Random Packings of Frictionless Particles. *Phys. Rev. Lett.*, 88(7):075507, January 2002. doi: 10.1103/PhysRevLett.88.075507. URL https://link.aps.org/doi/10.1103/PhysRevLett.88.075507.

[48] D. J. Durian. Foam Mechanics at the Bubble Scale. *Physical Review Letters*, 75(26): 4780–4783, December 1995. ISSN 0031-9007, 1079-7114. doi: 10.1103/PhysRevLett.75.4780. URL https://link.aps.org/doi/10.1103/PhysRevLett.75.4780.

[49] Matthieu Wyart. Marginal Stability Constrains Force and Pair Distributions at Random Close Packing. *Phys. Rev. Lett.*, 109(12):125502, September 2012. ISSN 0031-9007, 1079-7114. doi: 10.1103/PhysRevLett.109.125502. URL https://link.aps.org/doi/10.1103/PhysRevLett.109.125502.

[50] M. Wyart, S. R. Nagel, and T. A. Witten. Geometric origin of excess low-frequency vibrational modes in weakly connected amorphous solids. *EPL*, 72(3):486, September 2005. ISSN 0295-5075. doi: 10.1209/epl/i2005-10245-5. URL https://iopscience.iop.org/article/10.1209/epl/i2005-10245-5/meta. Publisher: IOP Publishing.

[51] M. Wyart. Scaling of phononic transport with connectivity in amorphous solids. *EPL*, 89(6): 64001, March 2010. ISSN 0295-5075, 1286-4854. doi: 10.1209/0295-5075/89/64001. URL https://epljournal.edpsciences.org/articles/epl/abs/2010/06/epl12551/epl12551.html.

[52] E. DeGiuli, E. Lerner, and M. Wyart. Theory of the Jamming Transition at Finite Temperature. *The Journal of Chemical Physics*, 142(16):164503, April 2015. ISSN 0021-9606, 1089-7690. doi: 10.1063/1.4918737. URL http://arxiv.org/abs/1501.06995. arXiv: 1501.06995.

[53] Patrick Charbonneau, Eric I. Corwin, Giorgio Parisi, and Francesco Zamponi. Universal Microstructure and Mechanical Stability of Jammed Packings. *Physical Review Letters*, 109 (20), November 2012. ISSN 0031-9007, 1079-7114. doi: 10.1103/PhysRevLett.109.205501. URL https://link.aps.org/doi/10.1103/PhysRevLett.109.205501.

[54] Patrick Charbonneau, Eric I. Corwin, Giorgio Parisi, and Francesco Zamponi. Jamming Criticality Revealed by Removing Localized Buckling Excitations. *Physical Review Letters*, 114(12), March 2015. ISSN 0031-9007, 1079-7114. doi: 10.1103/PhysRevLett.114.125504. URL https://link.aps.org/doi/10.1103/PhysRevLett.114.125504.

[55] Eric DeGiuli, Edan Lerner, Carolina Brito, and Matthieu Wyart. Force distribution affects vibrational properties in hard-sphere glasses. *PNAS*, 111(48):17054–17059, December 2014. ISSN 0027-8424, 1091-6490. doi: 10.1073/pnas.1415298111. URL http://www.pnas.org/content/111/48/17054.

[56] Edan Lerner, Gustavo Düring, and Matthieu Wyart. Low-energy non-linear excitations in sphere packings. *Soft Matter*, 9(34):8252–8263, August 2013. ISSN 1744-6848. doi: 10.1039/C3SM50515D. URL http://pubs.rsc.org/en/content/articlelanding/2013/sm/c3sm50515d.

[57] Atsushi Ikeda, Ludovic Berthier, and Giulio Biroli. Dynamic criticality at the jamming transition. *The Journal of Chemical Physics*, 138(12):12A507, March 2013. ISSN 0021-9606, 1089-7690. doi: 10.1063/1.4769251. URL http://aip.scitation.org/doi/10.1063/1.4769251.

[58] Carolina Brito and Matthieu Wyart. Geometric interpretation of previtrification in hard sphere liquids. *J. Chem. Phys.*, 131(2):024504, July 2009. ISSN 0021-9606. doi: 10.1063/1.3157261. URL https://aip.scitation.org/doi/abs/10.1063/1.3157261.

[59] Carl F. Schreck, Thibault Bertrand, Corey S. O'Hern, and M. D. Shattuck. Repulsive Contact Interactions Make Jammed Particulate Systems Inherently Nonharmonic. *Phys. Rev. Lett.*, 107(7):078301, August 2011. ISSN 0031-9007, 1079-7114. doi: 10.1103/PhysRevLett.107.078301. URL https://link.aps.org/doi/10.1103/PhysRevLett.107.078301.

[60] Silvio Franz, Giorgio Parisi, Pierfrancesco Urbani, and Francesco Zamponi. Universal spectrum of normal modes in low-temperature glasses. *Proceedings of the National Academy of Sciences*, 112(47):14539–14544, November 2015. ISSN 0027-8424, 1091-6490. doi: 10.1073/pnas.1511134112. URL http://www.pnas.org/lookup/doi/10.1073/pnas.1511134112.

[61] Hugo Jacquin, Ludovic Berthier, and Francesco Zamponi. Microscopic Mean-Field Theory of the Jamming Transition. *Phys. Rev. Lett.*, 106(13):135702, March 2011. doi: 10.1103/PhysRevLett.106.135702. URL https://link.aps.org/doi/10.1103/PhysRevLett.106.135702.

[62] Patrick Charbonneau, Eric I. Corwin, Giorgio Parisi, Alexis Poncet, and Francesco Zamponi. Universal Non-Debye Scaling in the Density of States of Amorphous Solids. *Phys. Rev. Lett.*, 117(4):045503, July 2016. doi: 10.1103/PhysRevLett.117.045503. URL https://link.aps.org/doi/10.1103/PhysRevLett.117.045503.

[63] Edan Lerner, Gustavo Düring, and Eran Bouchbinder. Statistics and Properties of Low-Frequency Vibrational Modes in Structural Glasses. *Physical Review Letters*, 117(3), July 2016. ISSN 0031-9007, 1079-7114. doi: 10.1103/PhysRevLett.117.035501.

[64] Corrado Rainone, Pierfrancesco Urbani, Hajime Yoshino, and Francesco Zamponi. Following the Evolution of Hard Sphere Glasses in Infinite Dimensions under External Perturbations: Compression and Shear Strain. *Phys. Rev. Lett.*, 114(1):015701, January 2015. ISSN 0031-9007, 1079-7114. doi: 10.1103/PhysRevLett.114.015701. URL https://link.aps.org/doi/10.1103/PhysRevLett.114.015701.

[65] Hajime Yoshino and Francesco Zamponi. Shear modulus of glasses: Results from the full replica-symmetry-breaking solution. *Phys. Rev. E*, 90(2):022302, August 2014. ISSN 1539-3755, 1550-2376. doi: 10.1103/PhysRevE.90.022302. URL https://link.aps.org/doi/10.1103/PhysRevE.90.022302.

[66] Giulio Biroli and Pierfrancesco Urbani. Breakdown of elasticity in amorphous solids. *Nature Phys*, 12(12):1130–1133, December 2016. ISSN 1745-2473, 1745-2481. doi: 10.1038/nphys3845. URL http://www.nature.com/articles/nphys3845.

[67] Pierfrancesco Urbani and Francesco Zamponi. Shear Yielding and Shear Jamming of Dense Hard Sphere Glasses. *Phys. Rev. Lett.*, 118(3):038001, January 2017. ISSN 0031-9007, 1079-7114. doi: 10.1103/PhysRevLett.118.038001. URL https://link.aps.org/doi/10.1103/PhysRevLett.118.038001.

[68] Ivo R. Peters, Sayantan Majumdar, and Heinrich M. Jaeger. Direct observation of dynamic shear jamming in dense suspensions. *Nature*, 532(7598):214–217, April 2016. ISSN 0028-0836, 1476-4687. doi: 10.1038/nature17167. URL http://www.nature.com/articles/nature17167.

[69] Giorgio Parisi, Itamar Procaccia, Corrado Rainone, and Murari Singh. Shear bands as manifestation of a criticality in yielding amorphous solids. *Proc Natl Acad Sci USA*, 114 (22):5577–5582, May 2017. ISSN 0027-8424, 1091-6490. doi: 10.1073/pnas.1700075114. URL http://www.pnas.org/lookup/doi/10.1073/pnas.1700075114.

[70] Jie Lin, Edan Lerner, Alberto Rosso, and Matthieu Wyart. Scaling description of the yielding transition in soft amorphous solids at zero temperature. *Proc Natl Acad Sci USA*, 111(40): 14382–14387, October 2014. ISSN 0027-8424, 1091-6490. doi: 10.1073/pnas.1406391111. URL http://www.pnas.org/lookup/doi/10.1073/pnas.1406391111.

[71] Misaki Ozawa, Ludovic Berthier, Giulio Biroli, Alberto Rosso, and Gilles Tarjus. Random critical point separates brittle and ductile yielding transitions in amorphous materials. *PNAS*, 115(26):6656–6661, June 2018. ISSN 0027-8424, 1091-6490. doi: 10.1073/pnas.1806156115. URL https://www.pnas.org/content/115/26/6656.

[72] Ke Chen, M. L. Manning, Peter J. Yunker, Wouter G. Ellenbroek, Zexin Zhang, Andrea J. Liu, and A. G. Yodh. Measurement of Correlations between Low-Frequency Vibrational Modes and Particle Rearrangements in Quasi-Two-Dimensional Colloidal Glasses. *Physical Review Letters*, 107(10), August 2011. ISSN 0031-9007, 1079-7114. doi: 10.1103/PhysRevLett.107.108301. URL https://link.aps.org/doi/10.1103/PhysRevLett.107.108301.

[73] C. A. Angell. Perspective on the glass transition. *Journal of Physics and Chemistry of Solids*, 49(8):863–871, January 1988. ISSN 0022-3697. doi: 10.1016/0022-3697(88)90002-9. URL http://www.sciencedirect.com/science/article/pii/0022369788900029.

[74] Ludovic Berthier and Giulio Biroli. Theoretical perspective on the glass transition and amorphous materials. *Reviews of Modern Physics*, 83(2):587–645, June 2011. ISSN 0034-6861, 1539-0756. doi: 10.1103/RevModPhys.83.587. URL https://link.aps.org/doi/10.1103/RevModPhys.83.587.

[75] Ning Xu, Matthieu Wyart, Andrea J. Liu, and Sidney R. Nagel. Excess Vibrational Modes and the Boson Peak in Model Glasses. *Phys. Rev. Lett.*, 98(17):175502, April 2007. doi: 10.1103/PhysRevLett.98.175502. URL https://link.aps.org/doi/10.1103/PhysRevLett.98.175502.

[76] P. Debye. Zur Theorie der spezifischen Wärmen. *Annalen der Physik*, 344(14):789–839, 1912. ISSN 1521-3889. doi: 10.1002/andp.19123441404. URL https://onlinelibrary.wiley.com/doi/abs/10.1002/andp.19123441404.

[77] R. C. Zeller and R. O. Pohl. Thermal Conductivity and Specific Heat of Noncrystalline Solids. *Phys. Rev. B*, 4(6):2029–2041, September 1971. doi: 10.1103/PhysRevB.4.2029. URL https://link.aps.org/doi/10.1103/PhysRevB.4.2029.

[78] U Buchenau, A Wischnewski, M Ohl, and E Fabiani. Neutron scattering evidence on the nature of the boson peak. *Journal of Physics: Condensed Matter*, 19(20):205106, May 2007. ISSN 0953-8984, 1361-648X. doi: 10.1088/0953-8984/19/20/205106. URL http://stacks.iop.org/0953-8984/19/i=20/a=205106?key=crossref.397821a99c56f9eb14641eea18a687be.

[79] P. W. Anderson, B. I. Halperin, and C. M. Varma. Anomalous low-temperature thermal properties of glasses and spin glasses. *The Philosophical Magazine: A Journal of Theoretical Experimental and Applied Physics*, 25(1):1–9, 1972. doi: 10.1080/14786437208229210. URL https://doi.org/10.1080/14786437208229210.

[80] Tsuneyoshi Nakayama. Boson peak and terahertz frequency dynamics of vitreous silica. *Reports on Progress in Physics*, 65(8):1195–1242, August 2002. ISSN 0034-4885. doi: 10.1088/0034-4885/65/8/203. URL http://stacks.iop.org/0034-4885/65/i=8/a=203?key=crossref.fbc6b86696cc37492f34d27141a8c439.

[81] Ke Chen, Wouter G. Ellenbroek, Zexin Zhang, Daniel T. N. Chen, Peter J. Yunker, Silke Henkes, Carolina Brito, Olivier Dauchot, Wim van Saarloos, Andrea J. Liu, and A. G. Yodh. Low-Frequency Vibrations of Soft Colloidal Glasses. *Physical Review Letters*, 105(2), July 2010. ISSN 0031-9007, 1079-7114. doi: 10.1103/PhysRevLett.105.025501. URL https://link.aps.org/doi/10.1103/PhysRevLett.105.025501.

[82] Le Yan, Eric DeGiuli, and Matthieu Wyart. On variational arguments for vibrational modes near jamming. *EPL*, 114(2):26003, April 2016. ISSN 0295-5075. doi: 10.1209/0295-5075/114/26003. URL https://doi.org/10.1209%2F0295-5075%2F114%2F26003.

[83] M. L. Manning and A. J. Liu. Vibrational Modes Identify Soft Spots in a Sheared Disordered Packing. *Phys. Rev. Lett.*, 107(10):108302, August 2011. ISSN 0031-9007, 1079-7114. doi: 10.1103/PhysRevLett.107.108302. URL https://link.aps.org/doi/10.1103/PhysRevLett.107.108302.

[84] V. Mazzacurati, G. Ruocco, and M. Sampoli. Low-frequency atomic motion in a model glass. *Europhys. Lett.*, 34(9):681–686, June 1996. ISSN 0295-5075, 1286-4854. doi: 10.1209/epl/i1996-00515-8. URL https://epljournal.edpsciences.org/articles/epl/abs/1996/18/34908/34908.html.

[85] N. Xu, V. Vitelli, A. J. Liu, and S. R. Nagel. Anharmonic and quasi-localized vibrations in jammed solids—Modes for mechanical failure. *EPL*, 90(5):56001, June 2010. ISSN 0295-5075. doi: 10.1209/0295-5075/90/56001. URL https://doi.org/10.1209%2F0295-5075%2F90%2F56001.

[86] Lijin Wang, Andrea Ninarello, Pengfei Guan, Ludovic Berthier, Grzegorz Szamel, and Elijah Flenner. Low-frequency vibrational modes of stable glasses. *Nature Communications*, 10(1):26, January 2019. ISSN 2041-1723. doi: 10.1038/s41467-018-07978-1. URL https://www.nature.com/articles/s41467-018-07978-1.

[87] Leonardo E. Silbert, Andrea J. Liu, and Sidney R. Nagel. Vibrations and Diverging Length Scales Near the Unjamming Transition. *Phys. Rev. Lett.*, 95(9):098301, August 2005. doi: 10.1103/PhysRevLett.95.098301. URL https://link.aps.org/doi/10.1103/PhysRevLett.95.098301.

[88] M. Baity-Jesi, V. Martín-Mayor, G. Parisi, and S. Perez-Gaviro. Soft Modes, Localization, and Two-Level Systems in Spin Glasses. *Phys. Rev. Lett.*, 115(26):267205, December 2015. doi: 10.1103/PhysRevLett.115.267205. URL https://link.aps.org/doi/10.1103/PhysRevLett.115.267205.

[89] Asaph Widmer-Cooper, Heidi Perry, Peter Harrowell, and David R. Reichman. Irreversible reorganization in a supercooled liquid originates from localized soft modes. *Nature Phys*, 4 (9):711–715, September 2008. ISSN 1745-2481. doi: 10.1038/nphys1025. URL https://www.nature.com/articles/nphys1025.

[90] Peter K. Morse, Sven Wijtmans, Merlijn van Deen, Martin van Hecke, and M. Lisa Manning. Two classes of events in sheared particulate matter. *arXiv:1907.10198 [cond-mat]*, July 2019. URL http://arxiv.org/abs/1907.10198. arXiv: 1907.10198.

[91] W. A. Phillips. Tunneling states in amorphous solids. *J Low Temp Phys*, 7(3):351–360, May 1972. ISSN 1573-7357. doi: 10.1007/BF00660072. URL https://doi.org/10.1007/BF00660072.

[92] Yu. M. Galperin, V. L. Gurevich, and D. A. Parshin. Theory of low-temperature thermal expansion of glasses. *Physical Review B*, 32(10):6873–6883, November 1985. ISSN 0163-1829. doi: 10.1103/PhysRevB.32.6873. URL https://link.aps.org/doi/10.1103/PhysRevB.32.6873.

[93] V G Karpov and D A Parshin. The thermal conductivity of glasses at temperatures below the Debye temperature. *Zh. Eksp. Teor. Fiz.*, (88):2212–2227, 1985.

[94] U. Buchenau, Yu. M. Galperin, V. L. Gurevich, D. A. Parshin, M. A. Ramos, and H. R. Schober. Interaction of soft modes and sound waves in glasses. *Physical Review B*, 46(5): 2798–2808, August 1992. ISSN 0163-1829, 1095-3795. doi: 10.1103/PhysRevB.46.2798. URL https://link.aps.org/doi/10.1103/PhysRevB.46.2798.

[95] V. L. Gurevich, D. A. Parshin, and H. R. Schober. Anharmonicity, vibrational instability, and the Boson peak in glasses. *Phys. Rev. B*, 67(9):094203, March 2003. doi: 10.1103/PhysRevB.67.094203. URL https://link.aps.org/doi/10.1103/PhysRevB.67.094203.

[96] Silvio Franz and Giorgio Parisi. The simplest model of jamming. *J. Phys. A: Math. Theor.*, 49 (14):145001, 2016. ISSN 1751-8121. doi: 10.1088/1751-8113/49/14/145001. URL http://stacks.iop.org/1751-8121/49/i=14/a=145001.

[97] Ada Altieri, Silvio Franz, and Giorgio Parisi. The jamming transition in high dimension: an analytical study of the TAP equations and the effective thermodynamic potential. *J. Stat. Mech.*, 2016(9):093301, September 2016. ISSN 1742-5468. doi: 10.1088/1742-5468/2016/09/093301. URL https://doi.org/10.1088%2F1742-5468%2F2016%2F09%2F093301.

[98] Ada Altieri. Higher-order corrections to the effective potential close to the jamming transition in the perceptron model. *Phys. Rev. E*, 97(1):012103, January 2018. doi: 10.1103/PhysRevE.97.012103. URL https://link.aps.org/doi/10.1103/PhysRevE.97.012103.

[99] Peter K. Morse and Eric I. Corwin. Geometric Signatures of Jamming in the Mechanical Vacuum. *Physical Review Letters*, 112(11), March 2014. ISSN 0031-9007, 1079-7114. doi: 10.1103/PhysRevLett.112.115701. URL https://link.aps.org/doi/10.1103/PhysRevLett.112.115701.

[100] Erik Bitzek, Pekka Koskinen, Franz Gähler, Michael Moseler, and Peter Gumbsch. Structural Relaxation Made Simple. *Phys. Rev. Lett.*, 97(17):170201, October 2006. doi: 10.1103/PhysRevLett.97.170201. URL https://link.aps.org/doi/10.1103/PhysRevLett.97.170201.

[101] Carl P. Goodrich, Andrea J. Liu, and Sidney R. Nagel. Finite-Size Scaling at the Jamming Transition. *Physical Review Letters*, 109(9), August 2012. ISSN 0031-9007, 1079-7114. doi: 10.1103/PhysRevLett.109.095704. URL https://link.aps.org/doi/10.1103/PhysRevLett.109.095704.

[102] Davide Fiocco, Giuseppe Foffi, and Srikanth Sastry. Encoding of Memory in Sheared Amorphous Solids. *Physical Review Letters*, 112(2), January 2014. ISSN 0031-9007, 1079-7114. doi: 10.1103/PhysRevLett.112.025702. URL https://link.aps.org/doi/10.1103/PhysRevLett.112.025702.

[103] Nathan C. Keim, Joseph D. Paulsen, Zorana Zeravcic, Srikanth Sastry, and Sidney R. Nagel. Memory formation in matter. *Reviews of Modern Physics*, 91(3), July 2019. ISSN 0034-6861, 1539-0756. doi: 10.1103/RevModPhys.91.035002. URL https://link.aps.org/doi/10.1103/RevModPhys.91.035002.

[104] Davide Fiocco, Giuseppe Foffi, and Srikanth Sastry. Oscillatory athermal quasistatic deformation of a model glass. *Physical Review E*, 88(2), August 2013. ISSN 1539-3755, 1550-2376. doi: 10.1103/PhysRevE.88.020301. URL https://link.aps.org/doi/10.1103/PhysRevE.88.020301.

[105] Patrick Charbonneau, Jorge Kurchan, Giorgio Parisi, Pierfrancesco Urbani, and Francesco Zamponi. Fractal free energy landscapes in structural glasses. *Nature Communications*, 5 (1), September 2014. ISSN 2041-1723. doi: 10.1038/ncomms4725. URL http://www.nature.com/articles/ncomms4725.

[106] Yuliang Jin and Hajime Yoshino. Exploring the complex free-energy landscape of the simplest glass by rheology. *Nat Commun*, 8(1):14935, April 2017. ISSN 2041-1723. doi: 10.1038/ncomms14935. URL http://www.nature.com/articles/ncomms14935.

[107] Asaf Szulc, Omri Gat, and Ido Regev. Forced deterministic dynamics on a random energy landscape: Implications for the physics of amorphous solids. *Phys. Rev. E*, 101(5):052616, May 2020. ISSN 2470-0045, 2470-0053. doi: 10.1103/PhysRevE.101.052616. URL https://link.aps.org/doi/10.1103/PhysRevE.101.052616.

[108] Monoj Adhikari and Srikanth Sastry. Memory formation in cyclically deformed amorphous solids and sphere assemblies. *Eur. Phys. J. E*, 41(9):105, September 2018. ISSN 1292-895X. doi: 10.1140/epje/i2018-11717-5. URL https://doi.org/10.1140/epje/i2018-11717-5.

[109] Andrea Ninarello, Ludovic Berthier, and Daniele Coslovich. Models and Algorithms for the Next Generation of Glass Transition Studies. *Phys. Rev. X*, 7(2):021039, June 2017. ISSN 2160-3308. doi: 10.1103/PhysRevX.7.021039. URL http://link.aps.org/doi/10.1103/PhysRevX.7.021039.

[110] Geert Kapteijns, Wencheng Ji, Carolina Brito, Matthieu Wyart, and Edan Lerner. Fast generation of ultrastable computer glasses by minimization of an augmented potential energy. *Phys. Rev. E*, 99(1):012106, January 2019. doi: 10.1103/PhysRevE.99.012106. URL https://link.aps.org/doi/10.1103/PhysRevE.99.012106. Publisher: American Physical Society.

[111] Yuliang Jin, Pierfrancesco Urbani, Francesco Zamponi, and Hajime Yoshino. A stability-reversibility map unifies elasticity, plasticity, yielding, and jamming in hard sphere glasses. *Sci. Adv.*, 4(12):eaat6387, December 2018. ISSN 2375-2548. doi: 10.1126/sciadv.aat6387. URL https://advances.sciencemag.org/lookup/doi/10.1126/sciadv.aat6387.

[112] Wei-Ting Yeh, Misaki Ozawa, Kunimasa Miyazaki, Takeshi Kawasaki, and Ludovic Berthier. Glass Stability Changes the Nature of Yielding under Oscillatory Shear. *Physical Review Letters*, 124(22), June 2020. ISSN 0031-9007, 1079-7114. doi: 10.1103/PhysRevLett.124.225502. URL https://link.aps.org/doi/10.1103/PhysRevLett.124.225502.

[113] Varda F. Hagh, Sidney R. Nagel, Andrea J. Liu, M. Lisa Manning, and Eric I. Corwin. Transient degrees of freedom and stability. *arXiv:2105.10846 [cond-mat]*, May 2021. URL http://arxiv.org/abs/2105.10846. arXiv: 2105.10846.

[114] Craig Maloney and Anaël Lemaître. Universal Breakdown of Elasticity at the Onset of Material Failure. *Phys. Rev. Lett.*, 93(19):195501, November 2004. doi: 10.1103/PhysRevLett.93.195501. URL https://link.aps.org/doi/10.1103/PhysRevLett.93.195501. Publisher: American Physical Society.

[115] Elisabeth Agoritsas. Mean-field dynamics of infinite-dimensional particle systems: global shear versus random local forcing. *J. Stat. Mech.*, 2021(3):033501, March 2021. ISSN 1742-5468. doi: 10.1088/1742-5468/abdd18. URL https://iopscience.iop.org/article/10.1088/1742-5468/abdd18.

[116] Peter K. Morse, Sudeshna Roy, Elisabeth Agoritsas, Ethan Stanifer, Eric I. Corwin, and M. Lisa Manning. A direct link between active matter and sheared granular systems. *Proc Natl Acad Sci USA*, 118(18):e2019909118, May 2021. ISSN 0027-8424, 1091-6490. doi: 10.1073/pnas.2019909118. URL http://www.pnas.org/lookup/doi/10.1073/pnas.2019909118.